

1 **Nocturnal Atmospheric Synergistic Oxidation Reduces the Formation of Low-volatility**  
2 **Organic Compounds from Biogenic Emissions**

3 Han Zang<sup>1</sup>, Zekun Luo<sup>1</sup>, Chenxi Li<sup>1</sup>, Ziyue Li<sup>1</sup>, Dandan Huang<sup>2,\*</sup>, Yue Zhao<sup>1,\*</sup>

4

5 <sup>1</sup>School of Environmental Science and Engineering, Shanghai Jiao Tong University, Shanghai,  
6 200240, China

7 <sup>2</sup>Shanghai Academy of Environmental Sciences, Shanghai, 200233, China

8 \*Correspondence: Yue Zhao (yuezhao20@sjtu.edu.cn); Dandan Huang (huangdd@saes.sh.cn);

9

10 **Abstract**

11 Volatile organic compounds (VOCs) are often subject to synergistic oxidation by different oxidants  
12 in the atmosphere. However, the exact synergistic oxidation mechanism of atmospheric VOCs and  
13 its role in particle formation remain poorly understood. In particular, the reaction kinetics of the key  
14 reactive intermediates, organic peroxy radicals (RO<sub>2</sub>), during synergistic oxidation is rarely studied.  
15 Here, we conducted a combined experimental and kinetic modelling study of the nocturnal  
16 synergistic oxidation of  $\alpha$ -pinene (the most abundant monoterpene) by O<sub>3</sub> and NO<sub>3</sub> radicals as well  
17 as its influences on the formation of highly oxygenated organic molecules (HOMs) and particles.  
18 We find that in the synergistic O<sub>3</sub> + NO<sub>3</sub> regime, where OH radicals are abundantly formed via  
19 decomposition of ozonolysis-derived Criegee intermediates, the production of C<sub>x</sub>H<sub>y</sub>O<sub>z</sub>-HOMs is  
20 substantially suppressed compared to that in the O<sub>3</sub>-only regime, mainly because of the termination  
21 depletion of  $\alpha$ -pinene RO<sub>2</sub> derived from ozonolysis and OH oxidation by those arising from NO<sub>3</sub>  
22 oxidation via cross reactions. Measurement-model comparisons further reveal that the cross-  
23 reaction rate constants of NO<sub>3</sub>-derived RO<sub>2</sub> with O<sub>3</sub>-derived RO<sub>2</sub> ~~is~~ are on average 10 – 100 times  
24 larger than those of NO<sub>3</sub>-derived RO<sub>2</sub> with OH-derived RO<sub>2</sub> ~~termination reactions between~~  
25 ~~ozonolysis and NO<sub>3</sub>-derived RO<sub>2</sub> are on average 10 – 100 times more efficient than those of OH-~~  
26 ~~and NO<sub>3</sub>-derived RO<sub>2</sub>~~. Despite a strong production of organic nitrates in the synergistic oxidation  
27 regime, the substantial decrease of C<sub>x</sub>H<sub>y</sub>O<sub>z</sub>-HOM formation leads to a significant reduction in  
28 ultralow- and extremely low-volatility organic compounds, which significantly inhibits the  
29 formation of new particles. This work provides valuable mechanistic and quantitative insights into  
30 the nocturnal synergistic oxidation chemistry of biogenic emissions and will help to better  
31 understand the formation of low-volatility organic compounds and particles in the atmosphere.  
32

### 33 **1. Introduction**

34 The Earth's atmosphere is a complex oxidizing environment in which multiple oxidants coexist.  
35 During the nighttime, NO<sub>3</sub> radicals (generated by the reaction of NO<sub>2</sub> and O<sub>3</sub>) and O<sub>3</sub> contribute  
36 significantly to the oxidation of volatile organic compounds (VOCs) (Huang et al., 2019), while  
37 during the daytime, the fast photolysis of NO<sub>3</sub> radicals and rapid photochemical formation of OH  
38 radicals and O<sub>3</sub> make the latter two the major oxidants for VOCs (Zhang et al., 2018). Therefore,  
39 the degradation of ambient VOCs is subject to concurrent oxidation by different oxidants. Gas-phase  
40 oxidation of VOCs from biogenic emissions (BVOCs) by these major atmospheric oxidants  
41 produces a key type of reactive intermediates, organic peroxy radicals (RO<sub>2</sub>), a portion of which can  
42 undergo fast autoxidation forming a class of highly oxygenated organic molecules (HOMs) with  
43 low volatilities (Jokinen et al., 2014; Mentel et al., 2015; Berndt et al., 2016; Zhao et al., 2018; Iyer  
44 et al., 2021; Shen et al., 2022; Ehn et al., 2014). HOMs typically contain six or more oxygen atoms,  
45 and plays a key role in the formation of atmospheric new particles and secondary organic aerosol  
46 (SOA) (Kirkby et al., 2016; Berndt et al., 2018a; Zhao et al., 2018; Ehn et al., 2014; Bianchi et al.,  
47 2019), which have important influences on air quality (Huang et al., 2014), public health (Pye et al.,  
48 2021), and Earth's radiative forcing (Shrivastava et al., 2017).

49 Due to the complexity of oxidation mechanisms of BVOCs, previous laboratory studies typically  
50 featured only one oxidant and a single SOA precursor (Berndt et al., 2016; Berndt, 2021; Clafin et  
51 al., 2018; Iyer et al., 2021; Boyd et al., 2015). However, the synergistic oxidation by different  
52 oxidants may significantly alter the fate of RO<sub>2</sub> intermediates, therefore influencing the formation  
53 of HOMs and SOA (Bates et al., 2022). Recently, a field study at a boreal forest site in Finland  
54 observed a series of nitrate-containing HOM-dimers from the coupled O<sub>3</sub> and NO<sub>3</sub> oxidation of  
55 monoterpenes (Zhang et al., 2020). At the same site, Lee et al. (2020) found that the synergistic  
56 oxidation of BVOCs by OH radicals and O<sub>3</sub> contributed to the largest fraction of SOA. These studies  
57 suggest that the synergistic oxidation of BVOCs by different oxidants plays an important role in the  
58 formation of HOMs and SOA in the atmosphere and highlight the needs to investigate the synergistic  
59 oxidation mechanisms of BVOCs for a better representation of atmospheric particle formation.

60 Several laboratory studies have attempted to address the role of synergistic oxidation of BVOCs in  
61 the formation of new particles and SOA (Kenseth et al., 2018; Inomata, 2021; Liu et al., 2022; Li et

62 al., 2024). Kenseth et al. (2018) identified a suite of dimer esters in flow tube experiments that can  
63 be only formed from the OH and O<sub>3</sub> synergistic oxidation of β-pinene. These dimers exhibit  
64 extremely low volatility and contributed 5.9 – 25.4% to the total β-pinene SOA. Similarly, Inomata  
65 (2021) found that the presence of OH radicals during α-pinene ozonolysis is a key factor for the  
66 production of low-volatility organic species and significantly promotes new particle formation  
67 (NPF). On the other hand, the addition of O<sub>3</sub> in the monoterpene photooxidation system also  
68 significantly increases the SOA mass yield (Liu et al., 2022). In addition, a recent chamber study  
69 by Bates et al. (2022) showed that the synergistic oxidation of α-pinene by NO<sub>3</sub> radicals and O<sub>3</sub> can  
70 significantly enhance the SOA yield compared to the NO<sub>3</sub> + α-pinene regime, which has nearly 0%  
71 SOA yield (Fry et al., 2014; Hallquist et al., 1999; Mutzel et al., 2021), and they revealed that the  
72 SOA yield in the NO<sub>3</sub> + O<sub>3</sub> oxidation system largely depends on the RO<sub>2</sub> fates. Most recently, Li et  
73 al. (2024) found that during α-pinene ozonolysis, the presence of nitrooxy-RO<sub>2</sub> radicals formed from  
74 NO<sub>3</sub> oxidation can significantly suppress the production of ultralow-volatility organic compounds  
75 (ULVOCs) and thereby NPF. These laboratory studies together provide growing evidence that  
76 synergistic oxidation of BVOCs by different oxidants have profound impacts on atmospheric  
77 particle formation. However, the specific synergistic mechanisms of different oxidants and  
78 oxidation pathways remain obscure. Although a few studies underscored the importance of the RO<sub>2</sub>  
79 fates (Bates et al., 2022; Li et al., 2024), the exact interactions between RO<sub>2</sub> species derived from  
80 different oxidants are still unclear, and quantitative constraints on the reaction rate of different RO<sub>2</sub>  
81 species are quite limited.

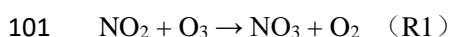
82 Here we conducted an investigation of the synergistic O<sub>3</sub> + NO<sub>3</sub> oxidation of α-pinene, one of the  
83 most abundant monoterpenes in the atmosphere, using a combination of laboratory experiments and  
84 detailed kinetic modelling, and focusing on the fate of RO<sub>2</sub> intermediates arising from different  
85 oxidation pathways. The α-pinene oxidation experiments were conducted in a custom-built flow  
86 reactor. The molecular composition of RO<sub>2</sub> species and HOMs in different oxidation regimes was  
87 characterized using a chemical ionization atmospheric pressure interface time-of-flight mass  
88 spectrometer (CI-APi-ToF) employing a nitrate ion source. The measured distributions of specific  
89 RO<sub>2</sub> and HOMs across different oxidation regimes were fitted with a kinetic model using Master  
90 Chemical Mechanisms (MCM v3.3.1) updated with recent advances of α-pinene RO<sub>2</sub> chemistry

91 (Wang et al., 2021; Iyer et al., 2021; Shen et al., 2022; Zang et al., 2023), which allows for  
92 quantitative constraints on RO<sub>2</sub> kinetics and synergistic oxidation mechanisms. Atmospheric  
93 relevance of the experimental results was evaluated by modelling the investigated oxidation  
94 chemistry under typical nocturnal atmospheric conditions.

## 95 **2. Materials and Methods**

### 96 **2.1 Flow tube experiments**

97 Experiments of  $\alpha$ -pinene oxidation in different regimes (i.e., synergistic O<sub>3</sub> + NO<sub>3</sub> oxidation vs. O<sub>3</sub>-  
98 only) were carried out under room temperature (298 K) and dry (relative humidity < 5%) conditions  
99 in a custom-built flow tube reactor (FTR, Figure S1). O<sub>3</sub> and NO<sub>2</sub> were added into a glass tube  
100 (Figure S1) to form NO<sub>3</sub> radical and its precursor N<sub>2</sub>O<sub>5</sub>:



103 O<sub>3</sub> was generated by passing a flow of ultra-high-purity (UHP) O<sub>2</sub> (Shanghai Maytor Special Gas  
104 Co., Ltd.) through a quartz tube housing a pen-ray mercury lamp (UV-S2, UVP Inc.) and its  
105 concentration was measured by an ozone analyzer (T400, API). NO<sub>2</sub> was obtained from a gas  
106 cylinder (15.6 ppm, Shanghai Weichuang Standard Gas Co., Ltd.). The initial NO<sub>2</sub> concentration in  
107 the flow tube was ~4.5 ppb. To prevent the titration of NO<sub>3</sub> radicals by NO, all the experiments  
108 were performed without the addition of NO. The total air flow in the NO<sub>3</sub> generation glass tube was  
109 0.6 L min<sup>-1</sup> and 0.4 L min<sup>-1</sup> for the gas-phase HOM and SOA formation experiments, respectively.  
110 The produced N<sub>2</sub>O<sub>5</sub> and NO<sub>3</sub> radicals, as well as the excessive O<sub>3</sub> were added into the FTR to initiate  
111  $\alpha$ -pinene oxidation. For the O<sub>3</sub>-only experiments, only O<sub>3</sub> was added into FTR.

112 The  $\alpha$ -pinene gas was generated by evaporating a defined volume of ~~their~~its liquid (99%, Sigma-  
113 Aldrich) into a cleaned and evacuated canister (SilcoCan, RESTEK), and then added into FTR  
114 through a movable injector at a flow rate of 22 – 108 mL min<sup>-1</sup>. The initial concentration of  $\alpha$ -pinene  
115 in the flow reactor ranged from 100 – 500 ppb. In some experiments, the gas of cyclohexane (~ 100  
116 ppm), which was generated by bubbling a gentle flow of UHP N<sub>2</sub> through its liquid (LC-MS grade,  
117 CNW), was added into the flow reactor as a scavenger of OH radicals formed from  $\alpha$ -pinene  
118 ozonolysis.

119 For experiments characterizing the formation of HOMs, the total air flow in the FTR was 10.8 L  
120  $\text{min}^{-1}$  and the residence time was 25 seconds. The short reaction time and the small amount of  
121 reacted  $\alpha$ -pinene (see Table S1) in these experiments prevented the formation of particles. For the  
122 experiments characterizing the formation of SOA particles, a larger FTR was used, with a total air  
123 flow of 5 L  $\text{min}^{-1}$  and a residence time of 180 seconds. A summary of the conditions including the  
124 simulated concentrations of  $\text{NO}_2$ ,  $\text{N}_2\text{O}_5$  and  $\text{NO}_3$  radicals, as well as the concentration of  $\alpha$ -pinene  
125 oxidized by each oxidant in different experiments are shown in Table S1.

126 The gas-phase  $\text{RO}_2$  radicals and closed-shell products were measured using a nitrate-based CI-API-  
127 ToF (abbreviated as nitrate-CIMS; Aerodyne Research, Inc.), which has been described in detail  
128 previously (Zang et al., 2023). A long ToF-MS with a mass resolution of  $\sim 10000$  Th/Th was used  
129 here. The mass spectra within the  $m/z$  range of 50-700 were analyzed using the tofTools package  
130 developed by Junninen et al. (2010) based on Matlab. The total ion counts (TIC), i.e., with values  
131 of  $(5.9 - 6.2) \times 10^4$  cps, are similar under different reaction conditions. In this study, we assume that  
132 the  $\text{C}_x\text{H}_y\text{O}_z$ -HOMs derived from ozonolysis and OH oxidation of  $\alpha$ -pinene exhibit the same  
133 sensitivity in nitrate-CIMS. However, the highly oxygenated organic nitrates may have a  
134 significantly lower sensitivity compared to the  $\text{C}_x\text{H}_y\text{O}_z$ -HOM counterparts, given that the  
135 substitution of -OOH or -OH groups by  $-\text{ONO}_2$  group in the molecule would reduce the number of  
136 H-bond donors, which is a key factor determining the sensitivity of nitrate-CIMS (Shen et al., 2022;  
137 Hyttinen et al., 2015). Recently, Li et al. (2024) used CI-Orbitrap with ammonium or nitrate reagent  
138 ions to detect oxygenated organic molecules in the synergistic  $\text{O}_3 + \text{NO}_3$  regime, and found that  
139 both the ion intensity of ONs and their signal contribution to the total dimers were much lower when  
140 using nitrate as reagent ions.

141 A scanning mobility particle sizer (SMPS, TSI), consisting of an electrostatic classifier (model  
142 3082), a condensation particle counter (model 3756), and a long or nano differential mobility  
143 analyzer (model 3081 and 3085), with a measurable size range of 4.61 – 156.8 nm and/or 14.6 –  
144 661.2 nm, respectively, was employed to monitor the formation of particles in the flow tube. During  
145 the HOM formation experiments, even under conditions with the highest initial  $\alpha$ -pinene  
146 concentration (500 ppb), only a tiny amount of particles was formed, with mass concentrations of  
147  $(6.4 \pm 1.6) \times 10^{-3}$  and  $(1.0 \pm 0.3) \times 10^{-2}$   $\mu\text{g m}^{-3}$  and number concentrations of  $574 \pm 138$  and  $256 \pm$

148 68 cm<sup>-3</sup> in the O<sub>3</sub>-only regime (Exp 5) and O<sub>3</sub> + NO<sub>3</sub> regimes (Exp 11), respectively. These results  
149 suggest that the formation of SOA particles in the HOM formation experiments is negligible and  
150 would have no significant influence on the fate of RO<sub>2</sub> and closed-shell products~~a differential~~  
151 ~~mobility analyzer (model 3081), and a condensation particle counter (model 3756), was employed~~  
152 ~~to monitor the formation of particles in different oxidation experiments.~~

## 153 2.2 Estimation of HOM volatility

154 A modified composition-activity method was used to estimate the saturation mass concentration  
155 (C\*) of HOMs in this study according to the approach developed by Li et al. (2016):

$$156 \log_{10}C^* = (n_C^0 - n_C)b_C - n_O b_O - 2 \frac{n_C n_O}{n_C + n_O} b_{CO} - n_N b_N - n_S b_S$$

157 where  $n_C^0$  is the reference carbon number;  $n_C$ ,  $n_O$ ,  $n_N$ , and  $n_S$  are the atom numbers of carbon,  
158 oxygen, nitrogen, and sulfur, respectively;  $b_C$ ,  $b_O$ ,  $b_N$ , and  $b_S$  are the contribution of each atom  
159 to  $\log_{10}C^*$ , respectively;  $b_{CO}$  is the carbon–oxygen nonideality (Donahue et al., 2011). These  $b$ -  
160 values were provided by Li et al. (2016).

161 It should be noted that the CHON compounds used in the data set by Li et al. (2016) are mostly  
162 amines, amides, and amino acids, and only contain a limited number of organic nitrates (0.07%).  
163 Since different types of CHON compounds have very different vapor pressures (Isaacman-Vanwertz  
164 and Aumont, 2021), this formula-based approach can be biased to estimate the C\* of organic nitrates.  
165 Considering that the –ONO<sub>2</sub> and –OH groups have similar impacts on vapor pressure and that the  
166 CHON species are predominantly organic nitrates in our study, all –ONO<sub>2</sub> groups are treated as OH  
167 groups during the estimation of vapor pressure (Daumit et al., 2013; Isaacman-Vanwertz and  
168 Aumont, 2021).

169 Gas-phase HOMs are grouped into five classes based on their  $\log_{10}C^*$  (Donahue et al., 2012;  
170 Bianchi et al., 2019; Schervish and Donahue, 2020), that is, ULVOCs ( $\log_{10}C^* < -8.5$ ), extremely  
171 low-volatility organic compounds (ELVOCs,  $-8.5 < \log_{10}C^* < -4.5$ ), low-volatility organic  
172 compounds (LVOCs,  $-4.5 < \log_{10}C^* < -0.5$ ), semi-volatile organic compounds (SVOCs,  $-0.5 <$   
173  $\log_{10}C^* < 2.5$ ), and intermediate-volatility organic compounds (IVOCs,  $2.5 < \log_{10}C^* < 6.5$ ).

## 174 2.3 Kinetic model simulations

175 Model simulations of specific RO<sub>2</sub> radicals and closed-shell HOMs formed in different oxidation  
176 regimes were performed to constrain the reaction kinetics and mechanisms using the Framework  
177 for 0-D Atmospheric Modeling (F0AM v4.1) (Wolfe et al., 2016), which employs MCM v3.3.1  
178 (Jenkin et al., 2015). The  $\alpha$ -pinene oxidation mechanism was updated with the state-of-the-art  
179 knowledge on the chemistry of RO<sub>2</sub> autoxidation and cross-reactions forming HOM monomers and  
180 dimers, respectively (Zhao et al., 2018; Wang et al., 2021; Iyer et al., 2021; Shen et al., 2022). The  
181 detailed updates have been described in our previous study (Zang et al., 2023). In particular, the  
182 formation and subsequent reactions of the ring-opened primary C<sub>10</sub>H<sub>15</sub>O<sub>4</sub>-RO<sub>2</sub>, the highly  
183 oxygenated acyl RO<sub>2</sub>, as well as the C<sub>10</sub>H<sub>15</sub>O<sub>2</sub>-RO<sub>2</sub> arising from H-abstraction by OH radicals  
184 during  $\alpha$ -pinene ozonolysis are included in the model according to recent studies (Iyer et al., 2021;  
185 Zhao et al., 2022; Zang et al., 2023; Shen et al., 2022).

186 To investigate the synergistic reactions of RO<sub>2</sub> derived from the oxidation of  $\alpha$ -pinene by different  
187 oxidants, we added the cross-reactions of the primary nitrooxy-RO<sub>2</sub> derived from NO<sub>3</sub> oxidation  
188 (<sup>NO<sub>3</sub></sup>RO<sub>2</sub>), i.e., C<sub>10</sub>H<sub>16</sub>NO<sub>5</sub>-RO<sub>2</sub>, with RO<sub>2</sub> derived from ozonolysis (<sup>Cl</sup>RO<sub>2</sub>) and OH oxidation  
189 (<sup>OH</sup>RO<sub>2</sub>). [Recently, Zhao et al. \(2018\) revealed the bulk rate constant for <sup>Cl</sup>RO<sub>2</sub> and <sup>OH</sup>RO<sub>2</sub> self/cross](#)  
190 [reactions to be  \$2 \times 10^{-12} \text{ cm}^3 \text{ molecule}^{-1} \text{ s}^{-1}\$ , and Bates et al. \(2022\) constrained the rate constant for](#)  
191 [<sup>NO<sub>3</sub></sup>RO<sub>2</sub> self/cross reactions to be  \$1 \times 10^{-13} - 1 \times 10^{-12} \text{ cm}^3 \text{ molecule}^{-1} \text{ s}^{-1}\$ . In the present study, the](#)  
192 [default rate constant for <sup>NO<sub>3</sub></sup>RO<sub>2</sub> + <sup>Cl</sup>RO<sub>2</sub> was set to  \$2 \times 10^{-12} \text{ cm}^3 \text{ molecule}^{-1} \text{ s}^{-1}\$ , the same to that for](#)  
193 [self/cross reactions of <sup>Cl</sup>RO<sub>2</sub> and <sup>OH</sup>RO<sub>2</sub>.](#) The ratio of the cross-reaction rate constant of <sup>NO<sub>3</sub></sup>RO<sub>2</sub> +  
194 <sup>Cl</sup>RO<sub>2</sub> to that of <sup>NO<sub>3</sub></sup>RO<sub>2</sub> + <sup>OH</sup>RO<sub>2</sub> was tuned to achieve a good measurement-model agreement for  
195 the distribution of specific RO<sub>2</sub> and HOMs across different oxidation regimes. [Recent studies](#)  
196 [suggested that the ROOR' dimer formation rates from the highly oxygenated RO<sub>2</sub> are fast](#) (Berndt  
197 et al., 2018b; Molteni et al., 2019). As a result, [a relatively high dimer formation branching ratio of](#)  
198 [50% was used for different RO<sub>2</sub> \(e.g., <sup>Cl</sup>RO<sub>2</sub>, <sup>OH</sup>RO<sub>2</sub>, <sup>NO<sub>3</sub></sup>RO<sub>2</sub>\) in this study.](#) With these default  
199 kinetic parameters, [the RO<sub>2</sub> bimolecular lifetimes were predicted to be 10.9 – 25.9 s in the O<sub>3</sub>-only](#)  
200 [regime and 8.4 – 11.8 s in the O<sub>3</sub> + NO<sub>3</sub> regime in the HOM formation experiments.](#) [Considering](#)  
201 [that the RO<sub>2</sub> cross-reaction kinetics remain highly uncertain, sensitivity analyses were performed to](#)  
202 [evaluate their influences on the results in this study \(see Section 3.2\).](#) Previous studies indicated that



203 the primary  $\text{NO}_3\text{RO}_2$  radicals arising from  $\alpha$ -pinene are prone to lose the nitrate group and form  
204 pinonaldehyde with high volatility (Kurtán et al., 2017; Fry et al., 2014). Therefore, we did not  
205 consider the autoxidation of primary  $\text{NO}_3\text{RO}_2$  in the model. Considering the presence of  $\text{NO}_2$  in the  
206 experiments, the reactions of  $\text{RO}_2 + \text{NO}_2 \rightleftharpoons \text{ROONO}_2$  were also included in the model (Zang et al.,  
207 2023).

### 208 3. Results and Discussion

#### 209 3.1 Molecular distribution of $\text{RO}_2$ and HOMs in the synergistic oxidation regime

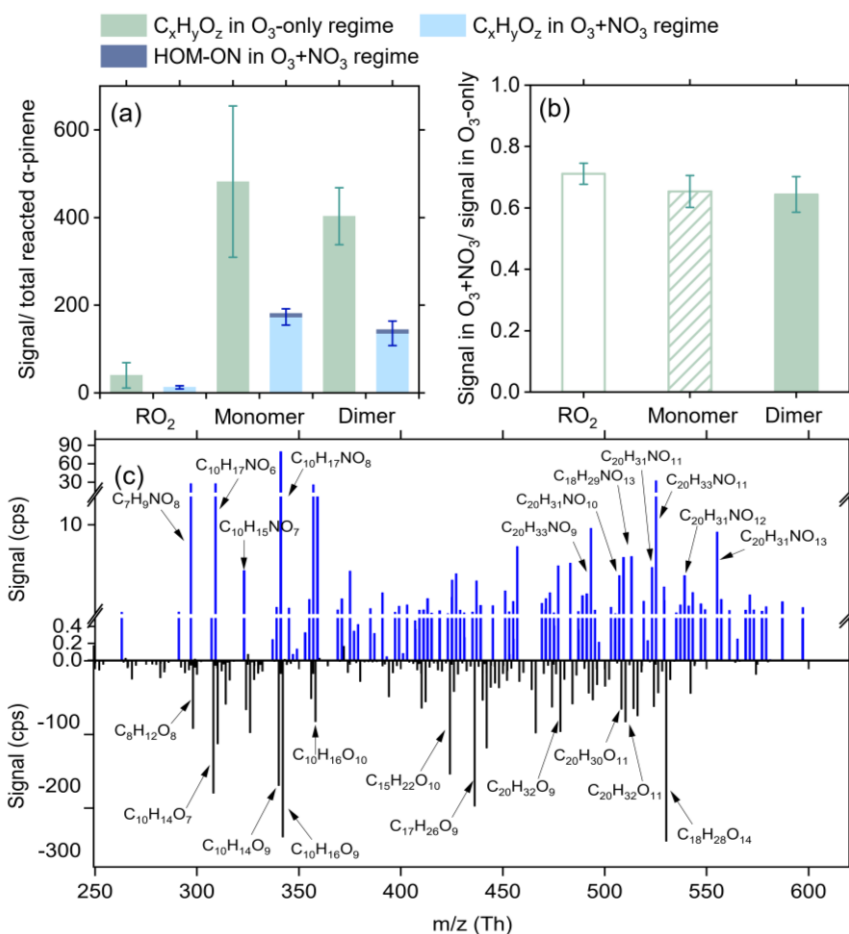
210 The ~~relative changes in the~~ abundance of gas-phase  $\text{RO}_2$  species and  $\text{C}_x\text{H}_y\text{O}_z$ -HOMs in ~~the~~  
211 ~~synergistic  $\text{O}_3 + \text{NO}_3$  oxidation of  $\alpha$ -pinene vs. versus the  $\text{O}_3$ -only regime are shown~~different  
212 oxidation regimes is shown in Figure 1a. The species signals are normalized by the total reacted  $\alpha$ -  
213 pinene in each ~~oxidation~~ regime. Compared to the  $\text{O}_3$ -only regime, the normalized signals of total  
214  $\text{RO}_2$  and HOMs decrease by 62 – 68% in the synergistic  $\text{O}_3 + \text{NO}_3$  regime. Although  $\text{NO}_3$  oxidation  
215 accounts for a considerable fraction of reacted  $\alpha$ -pinene in the synergetic oxidation regime, the  
216 signal contributions of HOM-ONs are not significant. This might be due to the low sensitivity of  
217 nitrate-CIMS to the ONs formed involving  $\text{NO}_3$  oxidation (see Section 2.1). The signals of  $\text{C}_x\text{H}_y\text{O}_z$ -  
218 HOMs significantly decrease by 29 – 36% in the synergistic  $\text{O}_3 + \text{NO}_3$  regime compared to those in  
219 the  $\text{O}_3$ -only regime (Figure 1a). Although there remain considerable uncertainties in instrument  
220 sensitivities to different compounds, sensitivity analyses suggest that varying the instrument CIMS  
221 sensitivities to  $\text{RO}_2$  and HOMs by a factor of 10 with different oxygenation levels would not  
222 significantly influence their relative distribution across different oxidation regimes (see Section S1  
223 for details).

224 Note that the initial concentrations of  $\alpha$ -pinene and  $\text{O}_3$  in the two oxidation regimes were the same.  
225 In addition, model simulations show that in the synergistic  ~~$\text{O}_3 + \text{NO}_3$  oxidation~~ regime, over 97% of  
226 OH radicals react with  $\alpha$ -pinene and the depletion of OH by  $\text{NO}_2$  is minor (0.2 – 1.3%). Also,  $\text{NO}_3$   
227 radicals almost entirely (over 98.5%) react with  $\alpha$ -pinene and their reaction with  $\text{RO}_2$  has negligible  
228 influence on the fate of  $\text{RO}_2$  (Figure S2). Meanwhile, the depletion of acyl  $\text{RO}_2$  by  $\text{NO}_2$  only leads  
229 to a small reduction (4 – 5% and 7 – 12%, respectively) in total  $\text{C}_x\text{H}_y\text{O}_z$ -HOM monomers and dimers  
230 in the synergistic regime compared to the  $\text{O}_3$ -only regime. As a result, the strong reduction in HOM  
231 formation due to the presence of  $\text{NO}_3$  oxidation is likely mainly due to (i) the fast competitive

232 consumption of  $\alpha$ -pinene by  $\text{NO}_3$  radicals, which leads to a reduction in the reacted  $\alpha$ -pinene by  $\text{O}_3$   
233 ( $\Delta[\alpha\text{-pinene}]_{\text{O}_3}$ , Figure S3) and thereby  $\text{C}_x\text{H}_y\text{O}_z$ -HOM signals, and (ii) the cross reactions of  $^{\text{Cl}}\text{RO}_2$   
234 or  $^{\text{OH}}\text{RO}_2$  with  $^{\text{NO}_3}\text{RO}_2$ , which suppress the autoxidation and self/cross reactions of  $^{\text{Cl}}\text{RO}_2$  and  $^{\text{OH}}\text{RO}_2$   
235 to form  $\text{C}_x\text{H}_y\text{O}_z$ -HOMs.

236 To quantify the contribution of cross reactions of  $^{\text{NO}_3}\text{RO}_2$  with  $^{\text{Cl}}\text{RO}_2/^{\text{OH}}\text{RO}_2$  to the suppressed  
237 formation of  $\text{C}_x\text{H}_y\text{O}_z$ -HOMs in the synergistic oxidation regime,  $\text{C}_x\text{H}_y\text{O}_z$ -HOM signals shown in  
238 Figure 1a are first~~ly~~ normalized to  $\Delta[\alpha\text{-pinene}]_{\text{O}_3}$  in each oxidation regime and then compared  
239 between different oxidation regimes (see Figure 1b).~~Therefore, the strong reduction in HOM~~  
240 ~~formation in the synergistic oxidation regime vs. the  $\text{O}_3$ -only regime is likely due to the following~~  
241 ~~two reasons. The first one is the fast competitive consumption of  $\alpha$ -pinene by  $\text{NO}_3$ -radicals, which~~  
242 ~~results in a reduction in the reacted  $\alpha$ -pinene by  $\text{O}_3$  ( $\Delta[\alpha\text{-pinene}]_{\text{O}_3}$ , Figure S2) and thereby the~~  
243 ~~formation of  $\text{C}_x\text{H}_y\text{O}_z$ -HOMs. The second reason is associated with the reactions of  $^{\text{NO}_3}\text{RO}_2$  with~~  
244  ~~$^{\text{Cl}}\text{RO}_2$  or  $^{\text{OH}}\text{RO}_2$  from  $\alpha$ -pinene, which suppresses the autoxidation and self/cross reactions of  $^{\text{Cl}}\text{RO}_2$~~   
245 ~~and  $^{\text{OH}}\text{RO}_2$  to form  $\text{C}_x\text{H}_y\text{O}_z$ -HOMs.~~

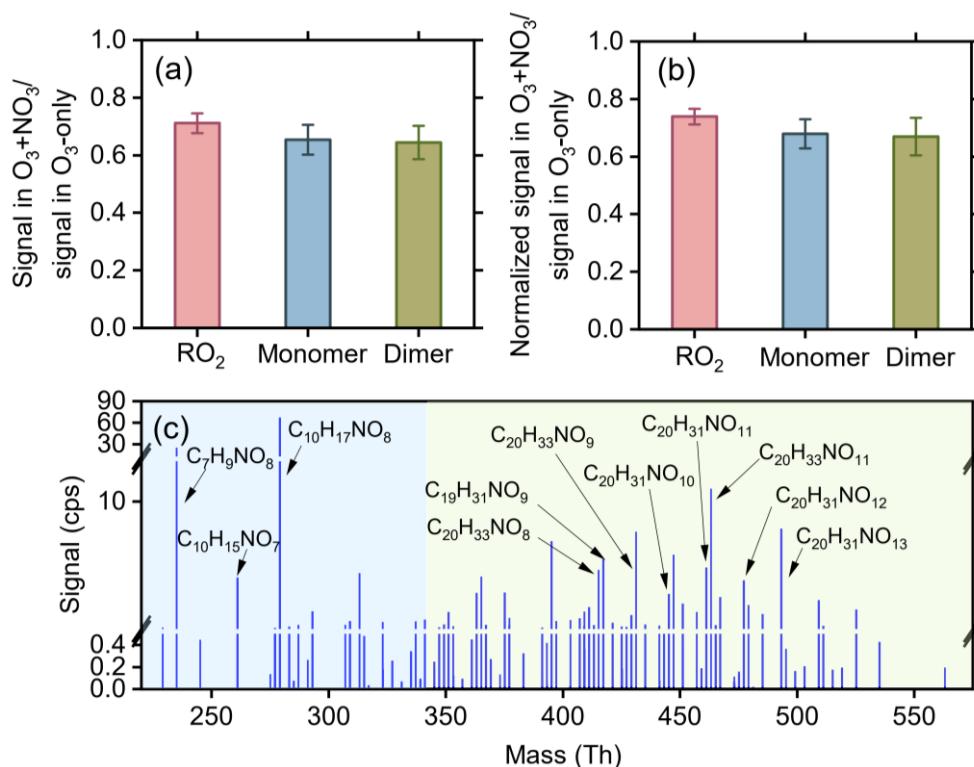
246 ~~To quantify the contribution of the synergistic  $\text{RO}_2$ -chemistry to the suppression of  $\text{C}_x\text{H}_y\text{O}_z$ -HOM~~  
247 ~~formation in the  $\text{O}_3 + \text{NO}_3$ -oxidation regime, the  $\text{C}_x\text{H}_y\text{O}_z$ -HOM signal ratios in Figure 1a are further~~  
248 ~~normalized to the ratio of  $\Delta[\alpha\text{-pinene}]_{\text{O}_3}$  in the synergistic oxidation regime vs. the  $\text{O}_3$ -only regime~~  
249 ~~(see Figure 1b).~~ Notably, after excluding the influence of reduced  $\Delta[\alpha\text{-pinene}]_{\text{O}_3}$ , the  $\text{C}_x\text{H}_y\text{O}_z$ -HOMs  
250 signals still drop by 24 – 32% in the  $\text{O}_3 + \text{NO}_3$  regime compared to those in the  $\text{O}_3$ -only regime,  
251 indicating a significant contribution of the coupled reactions between  $^{\text{NO}_3}\text{RO}_2$  and  $^{\text{Cl}}\text{RO}_2$  or  $^{\text{OH}}\text{RO}_2$   
252 to suppressed  $\text{C}_x\text{H}_y\text{O}_z$ -HOM formation.



253

254 [Figure 1 Distributions of RO<sub>2</sub> and HOMs in the O<sub>3</sub>-only and O<sub>3</sub> + NO<sub>3</sub> regimes. \(a\) Signals of total](#)  
 255 [RO<sub>2</sub>, as well as HOM monomers and dimers normalized by the reacted  \$\alpha\$ -pinene in each oxidation](#)  
 256 [regime \(Exps 1-5, 7-11\). \(b\) Relative changes in the normalized signals of C<sub>x</sub>H<sub>y</sub>O<sub>z</sub>-HOMs in the O<sub>3</sub>](#)  
 257 [+ NO<sub>3</sub> regime versus the O<sub>3</sub>-only regime. Ion signals are normalized to  \$\Delta\[\alpha\text{-pinene}\]\_{\text{O}\_3}\$  in each](#)  
 258 [oxidation regime to highlight the suppression effect of the synergistic chemistry between <sup>NO<sub>3</sub></sup>RO<sub>2</sub>](#)  
 259 [and <sup>Cl</sup>RO<sub>2</sub> or <sup>OH</sup>RO<sub>2</sub> on C<sub>x</sub>H<sub>y</sub>O<sub>z</sub>-HOM formation. \(c\) Difference mass spectrum between the two](#)  
 260 [oxidation regimes. The positive and negative peaks indicate the species with enhanced and](#)  
 261 [decreased formation in the O<sub>3</sub> + NO<sub>3</sub> regime compared to the O<sub>3</sub>-only regime, respectively.](#)

262



263

264 Figure 1. Distributions of RO<sub>2</sub> and HOMs in the synergistic O<sub>3</sub> + NO<sub>3</sub> regime. (a) Relative changes  
 265 in the signals of C<sub>x</sub>H<sub>y</sub>O<sub>z</sub>-RO<sub>2</sub> radicals, HOM monomers, and HOM dimers in the O<sub>3</sub> + NO<sub>3</sub> regime  
 266 compared to those in the O<sub>3</sub>-only regime (Exps 1-10). (b) Similar to (a), but with ion signals  
 267 normalized to Δ[α-pinene]<sub>O<sub>3</sub></sub> in each oxidation regime. (c) HOM nitrates measured in the O<sub>3</sub> + NO<sub>3</sub>  
 268 regime.

269 Figure 1c shows a difference mass spectrum highlighting the changes in species distribution  
 270 between the two oxidation regimes. Almost all C<sub>x</sub>H<sub>y</sub>O<sub>z</sub>-HOM species decrease significantly in the  
 271 O<sub>3</sub> + NO<sub>3</sub> regime compared to the O<sub>3</sub>-only regime. Besides, a large set of HOM-ON species are  
 272 formed, despite their relatively low signals. It should be noted that no obvious signals of highly  
 273 oxygenated <sup>NO<sub>3</sub></sup>RO<sub>2</sub> (C<sub>10</sub>H<sub>16</sub>NO<sub>x</sub>, x ≥ 6) were observed by nitrate-CIMS in the O<sub>3</sub> + NO<sub>3</sub> oxidation  
 274 system. One possible reason is that nitrate-CIMS exhibits relatively low sensitivity to the organic  
 275 nitrates. Secondly, the instrument's mass resolution is not high enough to differentiate the mass  
 276 closure between some of <sup>NO<sub>3</sub></sup>RO<sub>2</sub> and C<sub>x</sub>H<sub>y</sub>O<sub>z</sub>-HOMs with strong peaks (Table S3), limiting the  
 277 detection of <sup>NO<sub>3</sub></sup>RO<sub>2</sub> species. Furthermore, previous studies revealed that the primary <sup>NO<sub>3</sub></sup>RO<sub>2</sub>  
 278 radicals (i.e., C<sub>10</sub>H<sub>16</sub>NO<sub>5</sub>-RO<sub>2</sub>) in the α-pinene + NO<sub>3</sub> system mainly react to form pinonaldehyde  
 279 (Kurtén et al., 2017; Perraud et al., 2010). It is likely that only a very small amount of <sup>NO<sub>3</sub></sup>RO<sub>2</sub> can  
 280 undergo intramolecular H-shift/O<sub>2</sub> addition to form highly oxygenated <sup>NO<sub>3</sub></sup>RO<sub>2</sub>. It should be pointed  
 281 out that although the primary C<sub>10</sub>H<sub>16</sub>NO<sub>5</sub>-RO<sub>2</sub> species arising from NO<sub>3</sub> oxidation may not undergo

282 fast autoxidation, they tend to efficiently terminate  $^{\text{Cl}}\text{RO}_2$  and/or  $^{\text{OH}}\text{RO}_2$  and suppress the formation  
283 of  $\text{C}_x\text{H}_y\text{O}_z$ -HOMs.

284 As shown in Figure 1c, although several closed-shell monomeric HOM-ONs have been observed in  
285 the synergistic oxidation regime, only a few of them exhibit relatively high signals. Among them,  
286  $\text{C}_{10}\text{H}_{17}\text{NO}_8$  may be formed by the autoxidation of  $\text{C}_{10}\text{H}_{16}\text{NO}_6\text{-RO}_2$  derived from the intramolecular  
287 H-shift of primary  $^{\text{NO}_3}\text{RO}$  radicals ( $\text{C}_{10}\text{H}_{16}\text{NO}_4\text{-RO}$ ). In addition, although CI is a soft ionization  
288 method, the fragmentation of chemically labile species still occurs during the ionization in nitrate-  
289 CIMS. It is possible that some of dimeric HOM-ONs are fragmented to  $\text{C}_{10}\text{H}_{17}\text{NO}_8$  during nitrate-  
290 CIMS measurements. In a recent study by Li et al. (2024),  $\text{C}_{10}\text{H}_{17}\text{NO}_8$  was also identified during  
291 the synergistic oxidation of  $\alpha$ -pinene by  $\text{O}_3$  and  $\text{NO}_3$ . However, the exact origin of this species  
292 remains to be clarified.

293 The  $\text{C}_{20}$  dimers with only one nitrogen atom are very likely to be formed from the cross reactions  
294 of  $^{\text{Cl}}\text{RO}_2$  or  $^{\text{OH}}\text{RO}_2$  with  $^{\text{NO}_3}\text{RO}_2$ , which Figure 1e shows the signals of closed-shell monomeric and  
295 dimeric HOM nitrates (HOM-ONs) that were only observed in the synergistic  $\text{O}_3 + \text{NO}_3$  regime.  
296 Their specific formulas are listed in Table S2. These HOM-ONs mainly consist of  $\text{C}_{10}$  monomers  
297 and  $\text{C}_{20}$  dimers that only contain one nitrogen atom. The  $\text{C}_{20}$  HOM-ONs are believed to be formed  
298 from the cross reactions of  $^{\text{Cl}}\text{RO}_2$  and  $^{\text{OH}}\text{RO}_2$  with  $^{\text{NO}_3}\text{RO}_2$ . The substantial formation of these  
299 dimeric ONs provides direct evidence for the synergistic  $\text{RO}_2$  chemistry in the  $\text{O}_3 + \text{NO}_3$  regime.  
300 The  $\text{CHON}_2$  dimers were also observed in the  $\text{O}_3 + \text{NO}_3$  regime, despite their much lower signals  
301 than  $\text{CHON}$  dimers, which is different from the recent studies by Bates et al. (2022) and Li et al.  
302 (2024), which found  $\text{CHON}_2$  dimer account for an important fraction of the total dimer signals in  
303 the synergistic oxidation regime make important contribution to the total dimer signals. A potential  
304 explanation for this discrepancy is the difference in the instrument sensitivity in these studies  
305 (Section 2.1). In general, the nitrate-CIMS has lower sensitivities to ONs than to the  $\text{C}_x\text{H}_y\text{O}_z$ -HOM  
306 counterparts (Shen et al., 2022; Hyttinen et al., 2015). Bates et al. (2022) used  $\text{CF}_3\text{O}^-$  as the reagent  
307 ion of CIMS. Its sensitivity to ONs might be significantly higher than the nitrate ion. In addition, Li  
308 et al. (2024) observed a significantly lower signal contribution of  $\text{CHON}_2$  dimers using CI-Orbitrap  
309 with nitrate reagent ions than with ammonium ions. Despite both using nitrate reagent ions, the nitrate  
310 CI-Orbitrap in Li et al. (2024) possibly exhibits higher sensitivities to ONs than the nitrate-CIMS

311 [in our study.](#)

### 312 3.2 Synergistic reaction efficiencies of different RO<sub>2</sub> species

313 In the O<sub>3</sub> + NO<sub>3</sub> regime, synergistic reactions are likely to occur between <sup>Cl</sup>RO<sub>2</sub>, <sup>OH</sup>RO<sub>2</sub> and <sup>NO<sub>3</sub></sup>RO<sub>2</sub>.

314 Figure 2 shows the Δ[α-pinene]<sub>O<sub>3</sub></sub>-normalized signal ratios of specific C<sub>10</sub> RO<sub>2</sub> as well as their

315 related C<sub>x</sub>H<sub>y</sub>O<sub>z</sub>-HOM monomers and dimers in the synergistic O<sub>3</sub> + NO<sub>3</sub> regime vs. the O<sub>3</sub>-only

316 regime. [It should be noted that the second-generation oxidation processes are strongly inhibited by](#)

317 ~~an~~[the excess of α-pinene in this study, therefore](#) [the predominant type of RO<sub>2</sub> observed here is](#)

318 [primary RO<sub>2</sub>.](#) Model simulations show that the H-abstraction of α-pinene by OH radicals contributes

319 less than 2% to the formation of C<sub>10</sub>H<sub>15</sub>O<sub>x</sub>-RO<sub>2</sub> and related HOMs under different experimental

320 conditions (Figure [S3S5](#)). Therefore, C<sub>10</sub>H<sub>15</sub>O<sub>x</sub>-RO<sub>2</sub> observed in this study are primarily <sup>Cl</sup>RO<sub>2</sub>.

321 Notably, the <sup>Cl</sup>RO<sub>2</sub> (C<sub>10</sub>H<sub>15</sub>O<sub>x</sub>) and related C<sub>10</sub>H<sub>14</sub>O<sub>x</sub>-HOMs decrease by ~30 – 60% in the O<sub>3</sub> + NO<sub>3</sub>

322 regime (Figures 2 a, b), while the decreasing extent of <sup>OH</sup>RO<sub>2</sub> (C<sub>10</sub>H<sub>17</sub>O<sub>x</sub>) and related C<sub>10</sub>H<sub>18</sub>O<sub>x</sub>-

323 HOMs are significantly smaller (0 – 40%). In particular, some of the most oxygenated C<sub>10</sub>H<sub>17</sub>O<sub>x</sub>-

324 RO<sub>2</sub> and C<sub>10</sub>H<sub>18</sub>O<sub>x</sub>-HOMs (x ≥ 9) even increase unexpectedly in the synergistic oxidation regime.

325 For the C<sub>10</sub>H<sub>16</sub>O<sub>x</sub>-HOMs that can be derived from the [termination-self/cross](#) reactions of both <sup>Cl</sup>RO<sub>2</sub>

326 and <sup>OH</sup>RO<sub>2</sub>, their reductions are at a medium level. [Because of the very small contribution of acyl](#)

327 [RO<sub>2</sub> to the total C<sub>10</sub> RO<sub>2</sub> \(0.4%\) \(Zang et al., 2023\), their consumption by NO<sub>2</sub> leads to less than 2%](#)

328 [reduction in the C<sub>10</sub> <sup>Cl</sup>RO<sub>2</sub> signals. Therefore, ~~the more significantly larger~~ decrease in signals of](#)

329 <sup>Cl</sup>RO<sub>2</sub> and related HOMs as compared to the OH-derived ones [in the synergistic O<sub>3</sub> + NO<sub>3</sub> regime](#)

330 [is primarily due to](#) ~~indicates that in the synergistic O<sub>3</sub> + NO<sub>3</sub> regime, the more efficient cross~~

331 [reactions of <sup>NO<sub>3</sub></sup>RO<sub>2</sub> with <sup>Cl</sup>RO<sub>2</sub> than with <sup>OH</sup>RO<sub>2</sub> ~~the <sup>NO<sub>3</sub></sup>RO<sub>2</sub> species have a strong termination effect~~](#)

332 ~~on <sup>Cl</sup>RO<sub>2</sub> than on <sup>OH</sup>RO<sub>2</sub> (especially for the most oxygenated <sup>OH</sup>RO<sub>2</sub>).~~ Because a large amount of

333 <sup>Cl</sup>RO<sub>2</sub> is terminated by <sup>NO<sub>3</sub></sup>RO<sub>2</sub>, fewer <sup>Cl</sup>RO<sub>2</sub> are available to terminate <sup>OH</sup>RO<sub>2</sub>. As a result, more

334 <sup>OH</sup>RO<sub>2</sub> can undergo autoxidation to form highly oxygenated C<sub>10</sub>H<sub>17</sub>O<sub>x</sub>-RO<sub>2</sub> and C<sub>10</sub>H<sub>18</sub>O<sub>x</sub>-HOMs (x

335 ≥ 9), leading to an increase in signals of these species. Consistently, the signals of C<sub>20</sub> HOM dimers

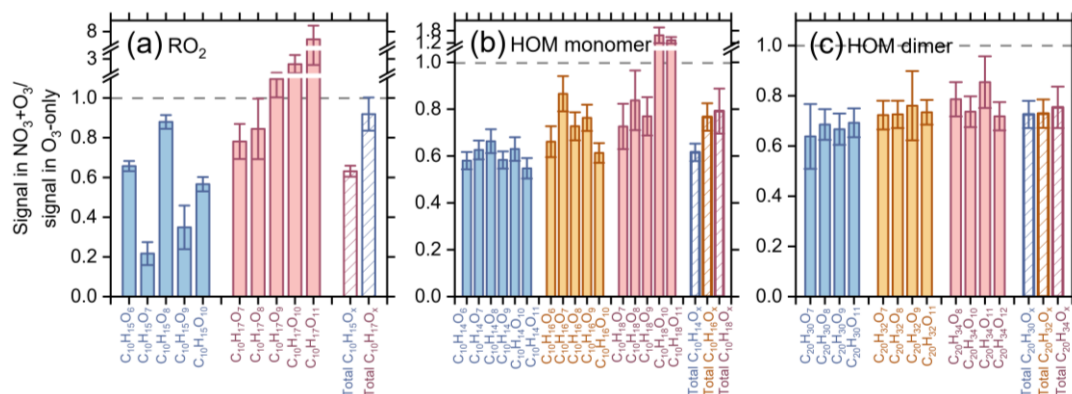
336 decrease by 20 – 40% in the O<sub>3</sub> + NO<sub>3</sub> regime compared to that in O<sub>3</sub>-only regime, and the signal

337 reduction of dimers (C<sub>20</sub>H<sub>30</sub>O<sub>x</sub>) formed by <sup>Cl</sup>RO<sub>2</sub> is slightly larger than that of the dimers (C<sub>20</sub>H<sub>34</sub>O<sub>x</sub>)

338 arising from <sup>OH</sup>RO<sub>2</sub> (Figure 2c). Note that the highly oxygenated C<sub>20</sub>H<sub>34</sub>O<sub>x</sub> dimers (x ≥ 13) that can

339 be formed from self/cross-reactions of C<sub>10</sub>H<sub>17</sub>O<sub>x</sub>-RO<sub>2</sub> (x ≥ 9) are not observed in this study, likely

340 due to their low abundance and the limitation of instrument sensitivity.



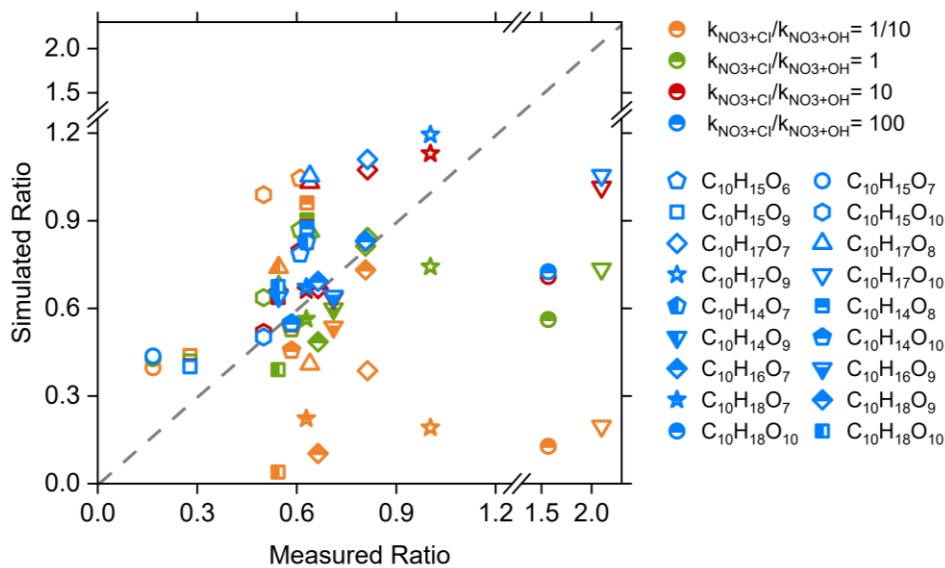
341  
342 Figure 2. Normalized signal ratios of (a) specific and total C<sub>10</sub>H<sub>15,17</sub>O<sub>x</sub>-RO<sub>2</sub> radicals, as well as their  
343 related (b) C<sub>10</sub> HOM monomers and (c) C<sub>20</sub> HOM dimers in the O<sub>3</sub> + NO<sub>3</sub> regime vs. the O<sub>3</sub>-only  
344 regime (Exps 1-10). Ion signals observed in each oxidation regime are normalized to Δ[α-pinene]<sub>O<sub>3</sub></sub>.

345 These above results are somewhat different from the most recent study by Li et al. (2024), which  
346 found that the measured C<sub>10</sub>H<sub>15</sub>O<sub>x</sub>-RO<sub>2</sub> increased slightly with NO<sub>3</sub> radicals while C<sub>10</sub>H<sub>17</sub>O<sub>5,7</sub>-RO<sub>2</sub>  
347 from OH chemistry decreased by a factor of 9. Li et al. (2024) indicated that additional C<sub>10</sub>H<sub>15</sub>O<sub>x</sub>  
348 could be produced from the H-abstraction pathway of NO<sub>3</sub> oxidation of α-pinene. However, in the  
349 monoterpene oxidation system, the rate constant for H-abstraction by NO<sub>3</sub> radicals is (4 – 10) × 10<sup>-</sup>  
350 17 cm<sup>3</sup> molecule<sup>-1</sup> s<sup>-1</sup>, which is 10<sup>3</sup> – 10<sup>4</sup> times lower than that for the NO<sub>3</sub> addition channel (Martinez  
351 et al., 1998). Besides, the subsequent reactions of RO<sub>2</sub> species formed from H-abstraction by NO<sub>3</sub>  
352 radicals should be very similar to those derived from H-abstraction by OH radicals, which was found  
353 not important for C<sub>x</sub>H<sub>y</sub>O<sub>z</sub>-HOM formation in the absence of NO (Zang et al., 2023). Therefore, the  
354 H-abstraction of α-pinene by NO<sub>3</sub> radicals would have negligible influence on C<sub>10</sub>H<sub>15</sub>O<sub>x</sub> formation.  
355 As Li et al. (2024) used a low α-pinene concentration and relatively high O<sub>3</sub> and NO<sub>3</sub> concentrations  
356 in their experiments, the secondary oxidation of aldehydes, such as the substantially formed  
357 pinonaldehyde, by NO<sub>3</sub> radicals might be important, which could contribute to the additional  
358 formation of C<sub>10</sub>H<sub>15</sub>O<sub>x</sub>-RO<sub>2</sub>. However, ~~in the present study~~ as noted above, the second-generation  
359 oxidation processes are strongly inhibited due to the excess of α-pinene in this study, therefore the  
360 formation of secondary C<sub>10</sub>H<sub>15</sub>O<sub>x</sub>-RO<sub>2</sub> is not important.

361 In addition, Li et al. (2024) reported that the fraction of α-pinene oxidized by OH radicals decreased  
362 from 44% in the O<sub>3</sub> oxidation system to 6% in the O<sub>3</sub> + NO<sub>3</sub> system, mainly due to the depletion of  
363 OH radicals by NO<sub>2</sub> and the competitive consumption of α-pinene by NO<sub>3</sub> radicals, which resulted

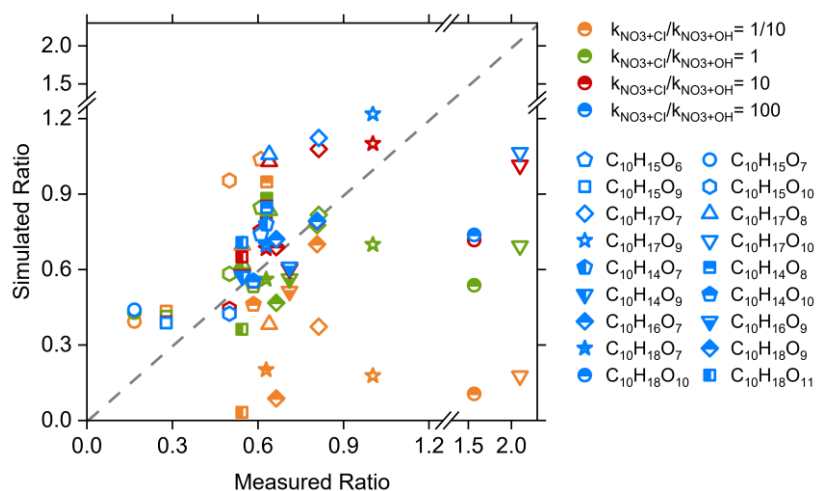
364 [in a significant decrease in C<sub>10</sub>H<sub>17</sub>O<sub>5,7</sub> radicals from OH chemistry as observed in their experiments.](#)  
 365 [However, in the present study, because of the excess of α-pinene, over 97% of OH radicals react](#)  
 366 [with α-pinene and the depletion of OH by NO<sub>2</sub> is minor \(0.2 – 1.3%\) in the O<sub>3</sub> + NO<sub>3</sub> regime. The](#)  
 367 [reduction in the reacted α-pinene by OH radicals is less than 10% compared to the O<sub>3</sub>-only regime.](#)  
 368 [As a result, a smaller decrease in C<sub>10</sub>H<sub>17</sub>O<sub>5,7</sub> radicals was observed in our study.](#)

369 To gain quantitative constraints on the relative reaction efficiency of <sup>NO<sub>3</sub></sup>RO<sub>2</sub> + <sup>Cl</sup>RO<sub>2</sub> vs. <sup>NO<sub>3</sub></sup>RO<sub>2</sub> +  
 370 <sup>OH</sup>RO<sub>2</sub> (i.e., k<sub>NO<sub>3</sub>+Cl</sub>/k<sub>NO<sub>3</sub>+OH</sub>), the signal ratios of C<sub>10</sub>-<sup>Cl</sup>RO<sub>2</sub> and <sup>OH</sup>RO<sub>2</sub> as well as their related C<sub>10</sub>  
 371 HOMs in the synergistic oxidation regime vs. the O<sub>3</sub>-only regime were predicted using a kinetic  
 372 model (see Section 2.3) with different k<sub>NO<sub>3</sub>+Cl</sub>/k<sub>NO<sub>3</sub>+OH</sub> ratios. Figure 3 shows a measurement-model  
 373 comparison of those signal ratios. When the ratio of k<sub>NO<sub>3</sub>+Cl</sub>/k<sub>NO<sub>3</sub>+OH</sub> is smaller than or equal to 1,  
 374 the simulated signal ratios of many RO<sub>2</sub> and HOMs differ significantly from the measured ratios,  
 375 especially for some C<sub>10</sub>H<sub>17</sub>O<sub>x</sub>-RO<sub>2</sub> and C<sub>10</sub>H<sub>18</sub>O<sub>x</sub>-HOMs. When the ratio of k<sub>NO<sub>3</sub>+Cl</sub>/k<sub>NO<sub>3</sub>+OH</sub> is 10 –  
 376 100, there is a good measurement-model agreement for most of RO<sub>2</sub> and HOMs. Therefore, we  
 377 conclude that the cross-reaction rate constants of <sup>NO<sub>3</sub></sup>RO<sub>2</sub> + <sup>Cl</sup>RO<sub>2</sub> are on average 10 – 100 times  
 378 larger than those for <sup>NO<sub>3</sub></sup>RO<sub>2</sub> + <sup>OH</sup>RO<sub>2</sub>. [This different RO<sub>2</sub> cross-reaction efficiency is the main](#)  
 379 [reason for the significantly larger decrease in the abundance of <sup>Cl</sup>RO<sub>2</sub> and related HOMs as](#)  
 380 [compared to the OH-derived ones \(see Figure 2\).](#)



381



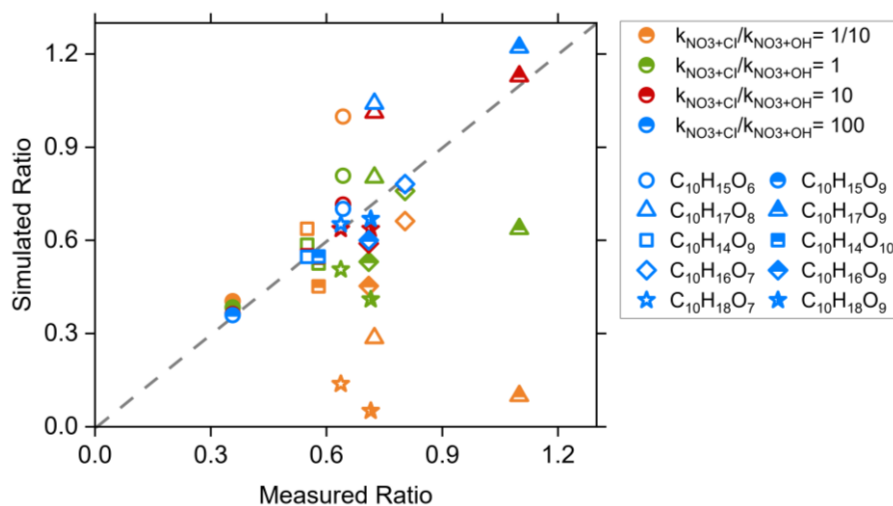


382

383 Figure 3. Measurement-model comparisons of the signal ratios of different C<sub>10</sub> RO<sub>2</sub> and HOMs in  
 384 the synergistic O<sub>3</sub> + NO<sub>3</sub> regime vs. the O<sub>3</sub>-only regime. The cross reaction rate constant of <sup>NO3</sup>RO<sub>2</sub>  
 385 + <sup>Cl</sup>RO<sub>2</sub> was set to 2 × 10<sup>-12</sup> cm<sup>3</sup> molecule<sup>-1</sup> s<sup>-1</sup> and the rate of <sup>NO3</sup>RO<sub>2</sub> + <sup>OH</sup>RO<sub>2</sub> was varied from 2 ×  
 386 10<sup>-11</sup> cm<sup>3</sup> molecule<sup>-1</sup> s<sup>-1</sup> to 2 × 10<sup>-14</sup> cm<sup>3</sup> molecule<sup>-1</sup> s<sup>-1</sup> in the model.

387 As a competitive reaction pathway, the autoxidation rates of RO<sub>2</sub> can affect the extent to which RO<sub>2</sub>  
 388 cross-reactions influence the RO<sub>2</sub> fate and HOM formation. Therefore, sensitivity analyses of the  
 389 autoxidation rate of RO<sub>2</sub> were conducted to evaluate its influence on the changes of RO<sub>2</sub> and related  
 390 HOM concentrations in the synergistic O<sub>3</sub> + NO<sub>3</sub> regime vs. the O<sub>3</sub>-only regime (Figure S4S7). In  
 391 these analyses, a k<sub>NO3+Cl</sub>/k<sub>NO3+OH</sub> ratio of 10 was used according to the above discussions. As the  
 392 autoxidation rate of <sup>OH</sup>RO<sub>2</sub> increases from 0.28 to 10 s<sup>-1</sup>, corresponding to the rate range reported in  
 393 previous studies (Berndt et al., 2016; Zhao et al., 2018; Xu et al., 2019), the simulated reduction of  
 394 highly oxygenated <sup>OH</sup>RO<sub>2</sub> and related C<sub>10</sub>H<sub>18</sub>O<sub>x</sub>-HOMs in the synergistic O<sub>3</sub> + NO<sub>3</sub> regime exhibits  
 395 a slight decrease (< 9%) but still agrees reasonably well with the measured value (Figures S4S7 a-  
 396 d). Considering that the autoxidation rates of <sup>Cl</sup>RO<sub>2</sub> used in the model approach their upper limits  
 397 reported in the literature, i.e., ~1 s<sup>-1</sup> for the butyl ring-opened C<sub>10</sub>H<sub>15</sub>O<sub>4</sub>-RO<sub>2</sub> (Iyer et al., 2021) and  
 398 relatively smaller rates for ring-retained C<sub>10</sub>H<sub>15</sub>O<sub>4</sub>-RO<sub>2</sub> (0.02 – 0.29 s<sup>-1</sup>, see Scheme S1) (Zhao et  
 399 al., 2021), we also lowered the autoxidation rate constants of <sup>Cl</sup>RO<sub>2</sub> by a factor of 10 to see its  
 400 influence on RO<sub>2</sub> and HOM distribution in the O<sub>3</sub> + NO<sub>3</sub> regime. The simulated reduction of <sup>Cl</sup>RO<sub>2</sub>  
 401 and C<sub>10</sub>H<sub>14</sub>O<sub>x</sub>-HOMs in this case decreases by 10 – 16% (Figures S4S7 e-h), while that of C<sub>10</sub>H<sub>16</sub>O<sub>x</sub>-  
 402 HOMs increases by up to 30% (Figures S4S7 i, j). However, the simulated results are still close to  
 403 the measured values. These sensitivity analyses suggest that the uncertainty in the autoxidation rates  
 404 of <sup>OH</sup>RO<sub>2</sub> and <sup>Cl</sup>RO<sub>2</sub> could slightly affect the simulated distribution of RO<sub>2</sub> and HOMs across

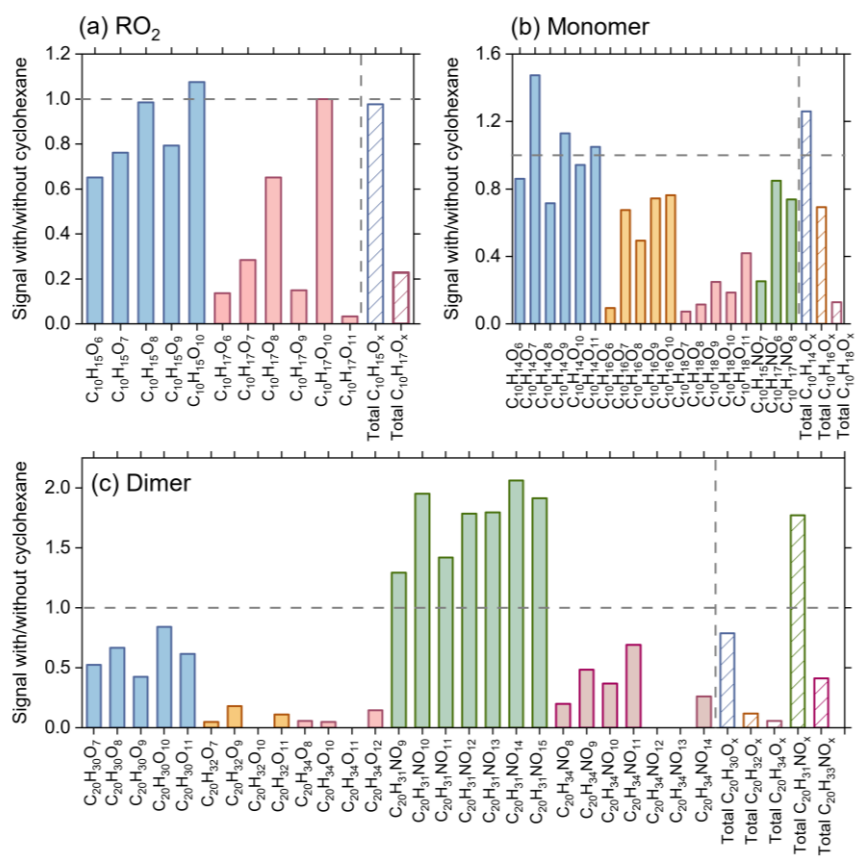
405 different oxidation regimes but not significantly change the  $k_{\text{NO}_3+\text{Cl}}/k_{\text{NO}_3+\text{OH}}$  ratio obtained in this  
 406 study. Further sensitivity analyses on the rate constant and dimer formation branching ratio of  $\text{RO}_2$   
 407 cross reactions indicate that the uncertainties in these reaction kinetics do not alter the conclusion  
 408 regarding the  $k_{\text{NO}_3+\text{Cl}}/k_{\text{NO}_3+\text{OH}}$  ratio either (see details in Sections S2 and S3).



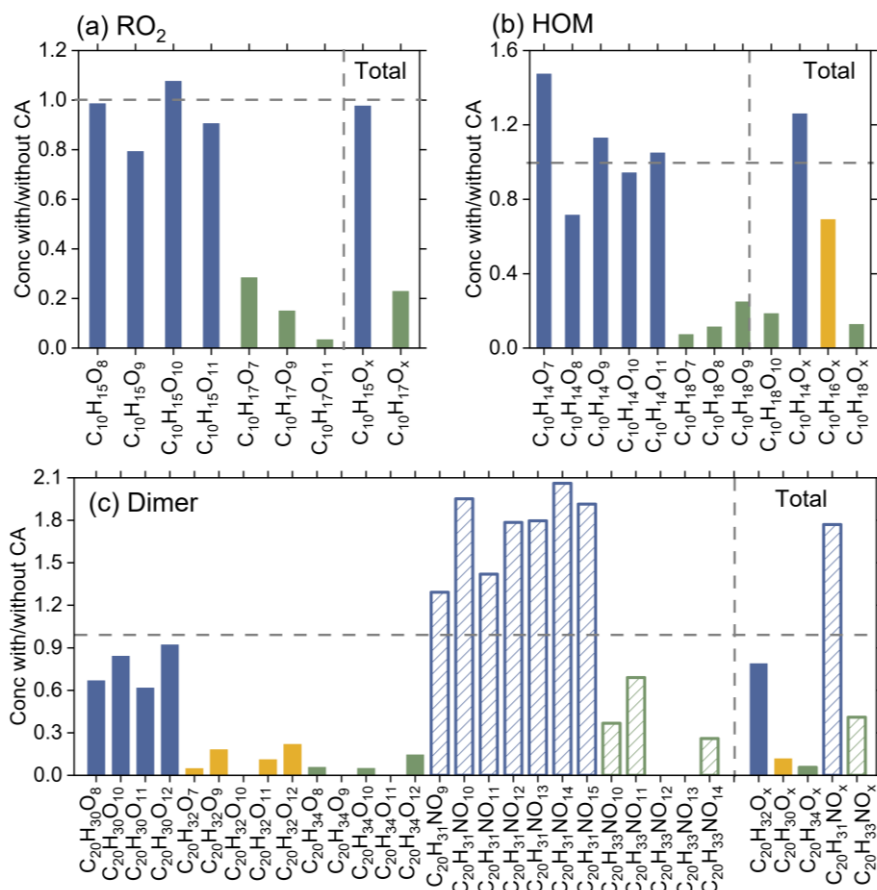
409

410 Cyclohexane was added in some experiments as an OH scavenger to elucidate the role of  $^{\text{OH}}\text{RO}_2$   
 411 chemistry in HOM formation in the  $\text{O}_3 + \text{NO}_3$  regime. In the presence of cyclohexane,  $^{\text{OH}}\text{RO}_2$   
 412 ( $\text{C}_{10}\text{H}_{17}\text{O}_x$ ) and related HOM monomers ( $\text{C}_{10}\text{H}_{18}\text{O}_x$ ) and dimers ( $\text{C}_{20}\text{H}_{32}\text{O}_x$  and  $\text{C}_{20}\text{H}_{34}\text{O}_x$ ) decrease  
 413 by more than 80% (Figure 4), while  $^{\text{Cl}}\text{RO}_2$  ( $\text{C}_{10}\text{H}_{15}\text{O}_x$ ) and related HOM monomers ( $\text{C}_{10}\text{H}_{14}\text{O}_x$ ) and  
 414 dimers ( $\text{C}_{20}\text{H}_{30}\text{O}_x$ ) only decrease slightly (< 30%), in a good agreement with previous measurements  
 415 (Zhao et al., 2018; Zang et al., 2023). The  $\text{C}_{10}\text{H}_{16}\text{O}_x$  species, which can arise from both  $^{\text{Cl}}\text{RO}_2$  and  
 416  $^{\text{OH}}\text{RO}_2$ , exhibit a medium reduction (Figure 4b). It is interesting to note that with the addition of  
 417 cyclohexane, there is a significant increase in  $\text{C}_{20}\text{H}_{31}\text{NO}_x$ , which are formed from the cross-  
 418 reactions of  $^{\text{Cl}}\text{RO}_2$  with  $^{\text{NO}_3}\text{RO}_2$ . Such an enhanced production of  $\text{C}_{20}\text{H}_{31}\text{NO}_x$  as compared to the  
 419 slightly decreased formation of  $\text{C}_{20}\text{H}_{30}\text{O}_x$  indicates that the  $^{\text{Cl}}\text{RO}_2 + ^{\text{NO}_3}\text{RO}_2$  reactions are competitive  
 420 compared to the  $^{\text{Cl}}\text{RO}_2 + ^{\text{Cl}}\text{RO}_2$  and  $^{\text{Cl}}\text{RO}_2 + ^{\text{OH}}\text{RO}_2$  reactionsthe cross-reaction of  $^{\text{Cl}}\text{RO}_2 + ^{\text{NO}_3}\text{RO}_2$  is  
 421 fast compared to that of  $^{\text{Cl}}\text{RO}_2 + ^{\text{Cl}}\text{RO}_2$  and  $^{\text{Cl}}\text{RO}_2 + ^{\text{OH}}\text{RO}_2$ . As a result, when the  $^{\text{OH}}\text{RO}_2$  are depleted,  
 422 the  $^{\text{Cl}}\text{RO}_2$  that are supposed to react with  $^{\text{OH}}\text{RO}_2$ , efficiently react with  $^{\text{NO}_3}\text{RO}_2$  to form  $\text{C}_{20}\text{H}_{31}\text{NO}_x$ ,  
 423 leading to the increase in  $\text{C}_{20}\text{H}_{31}\text{NO}_x$  signals. Consistent with the experimental measurements, the  
 424 model simulations show that the concentrations of  $\text{C}_{20}\text{H}_{31}\text{NO}_x$  in the  $\text{O}_3 + \text{NO}_3$  regime increase with  
 425 the addition of cyclohexane as an OH scavenger (Figure S9). However, the simulated enhancement

426 [is slightly lower than the measurements, which might be due to the uncertainties in the RO<sub>2</sub> cross-](#)  
 427 [reaction kinetics in the model.](#)



428



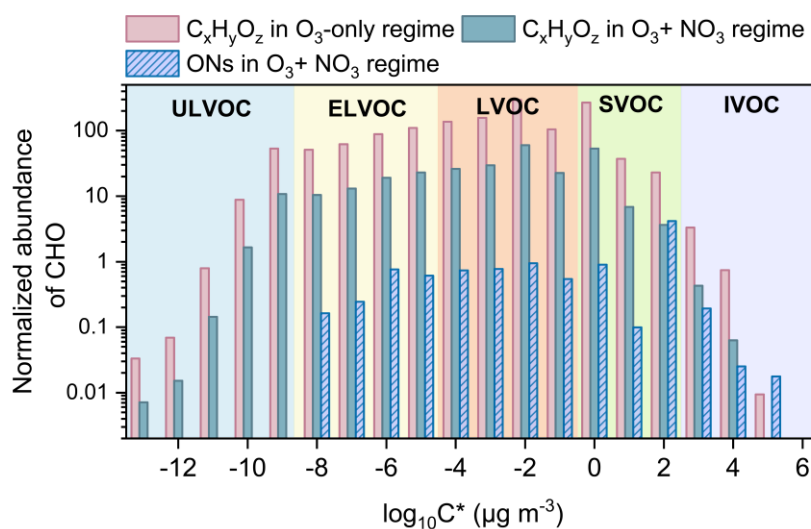
429

430 Figure 4. Relative changes in signals of (a)  $C_{10}$   $RO_2$ , (b)  $C_{10}$  HOMs, and (c)  $C_{20}$  dimers due to the  
 431 addition of 100 ppm cyclohexane as an OH scavenger derived in the synergistic  $O_3 + NO_3$  regime  
 432 (Exps 6-7 and 12).

### 433 3.3 Influence of synergistic oxidation on low-volatility organics and particle formation

434 Compared to the  $O_3$ -only regime, there ~~is~~<sup>are</sup> a remarkable reduction in  $C_xH_yO_z$ -HOMs and a strong  
 435 formation of HOM-ONs due to the ~~termination reactions~~<sup>efficient cross reactions</sup> between  $NO_3RO_2$   
 436 and  $^ClRO_2$  ~~or~~ <sup>$OHRO_2$</sup>  in the synergistic oxidation regime. This significant change in HOM  
 437 composition and abundance would alter the volatility distribution of HOMs and influence the  
 438 formation of particles. The volatilities of HOMs formed in the two oxidation regimes are estimated  
 439 using a modified composition-activity method (see Section 2.2) and shown in Figure 5. The  
 440 abundance of  $C_xH_yO_z$ -HOMs characterized as ULVOCs and ELVOCs decreases considerably in the  
 441 synergistic  $O_3 + NO_3$  regime compared to the  $O_3$ -only regime (Figure 5a), in agreement with the  
 442 very recent observations by Li et al. (2024) who found that the presence of  $NO_3$  radicals during  $\alpha$ -  
 443 pinene ozonolysis significantly reduced the abundance of ULVOCs. Although substantial amounts  
 444 of HOM-ONs are formed in the  $O_3 + NO_3$  regime, they generally have higher volatilities (i.e.,

445 characterized as ELVOCs to IVOCs) (Figure 5b). ~~In addition, the total abundance of newly formed~~  
 446 ~~HOM-ONs characterized as ELVOCs in the synergistic O<sub>3</sub> + NO<sub>3</sub> regime is significantly lower than~~  
 447 ~~the reduced formation of ultra and extremely low volatility C<sub>x</sub>H<sub>y</sub>O<sub>z</sub>-HOMs.~~ Therefore, the  
 448 synergistic O<sub>3</sub> + NO<sub>3</sub> oxidation of α-pinene significantly reduces the formation of ULVOCs and  
 449 increases the overall volatility of total HOMs.

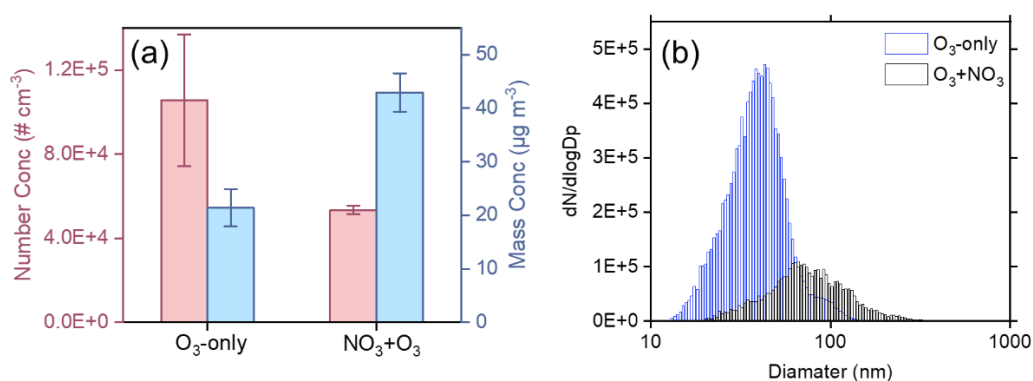


450  
 451 Figure 5. Volatility distribution of C<sub>x</sub>H<sub>y</sub>O<sub>z</sub>-HOMs and HOM-ONs formed in the O<sub>3</sub> + NO<sub>3</sub> regime  
 452 and O<sub>3</sub>-only regime (Exps 1, 6). Ion signals in each oxidation regime are normalized to the  
 453 corresponding total reacted α-pinene.

454 Figure 6a shows the particle number and mass concentrations formed in the two oxidation regimes  
 455 in SOA formation experiments (Table S1, Exps 13, 14). The particle number concentration decreases  
 456 by more than 50% whereas the particle mass concentration increases by a factor of 2 in the  
 457 synergistic O<sub>3</sub> + NO<sub>3</sub> regime, compared to that in the O<sub>3</sub>-only regime. The presence of NO<sub>3</sub> radicals  
 458 during α-pinene ozonolysis reduces the abundance of ULVOCs, which are the key species driving  
 459 particle nucleation, thereby leading to a reduction in the particle number concentration in the O<sub>3</sub> +  
 460 NO<sub>3</sub> regime. On the other hand, substantial formation of HOM-ONs is expected from the cross  
 461 reactions of <sup>NO3</sup>RO<sub>2</sub> with <sup>C</sup>RO<sub>2</sub> and <sup>OH</sup>RO<sub>2</sub> in the synergistic oxidation regime (Li et al., 2024; Bates  
 462 et al., 2022), although their signals are relatively low due to the low sensitivity of nitrate-CIMS to  
 463 ONs in this study. The newly formed HOM-ONs have relatively higher volatilities and are  
 464 inefficient in initiating particle nucleation, but they are able to partition into the formed particles  
 465 and contribute to the particle mass growth. Meanwhile, as the particle number concentration  
 466 decreases drastically in the synergistic oxidation regime, more condensable vapors are available for

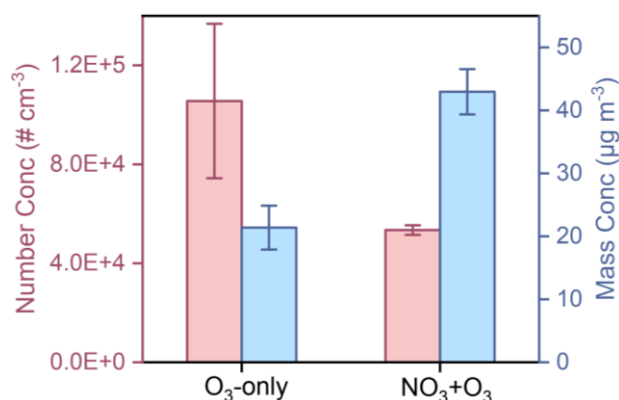
467 [each particle to grow to larger sizes \(Figure 6b\), which would in turn favor the condensation of more](#)  
 468 [volatile organic species including ONs due to the reduced curvature effect of the larger particles,](#)  
 469 [ultimately resulting in an increase in SOA mass concentrations.](#)

470 [Recently, Bates et al. \(2022\) also found that in chamber experiments with seed particles, the SOA](#)  
 471 [mass yields were significantly higher during  \$\alpha\$ -pinene oxidation by  \$O\_3 + NO\_3\$  than during ozonolysis,](#)  
 472 [mainly due to the substantial formation and condensation of ON dimers. However, in the absence](#)  
 473 [of seed particles, synergistic  \$O\_3 + NO\_3\$  oxidation of  \$\alpha\$ -pinene does not nucleate in their study. This](#)  
 474 [phenomenon might be due to the high concentrations of  \$NO\_2\$  \(72 ppb\) and  \$O\_3\$  \(102 ppb\) as well as](#)  
 475 [the relatively low concentration of  \$\alpha\$ -pinene \(27 ppb\) in their experiments. As indicated by Bates et](#)  
 476 [al. \(2022\),](#) under this conditions  $NO_3$  radicals were substantially formed and contributed to a  
 477 dominant fraction (75%) of  $\alpha$ -pinene oxidation, which strongly inhibited the production of low-  
 478 volatility species and particle nucleation. ~~The reduced particle number concentration in the  $O_3 +$~~   
 479  ~~$NO_3$  regime is ascribed to the suppressed formation of ULVOCs, which are the key species driving~~  
 480 ~~the particle nucleation (Simon et al., 2020; Schervish and Donahue, 2020). However, although the~~  
 481 ~~newly formed HOM ONs with relatively higher volatilities are inefficient in initiating particle~~  
 482 ~~nucleation, they are able to partition into the formed particles and contribute significantly to the~~  
 483 ~~particle mass growth. This result is consistent with a recent chamber study which found that the~~  
 484 ~~SOA mass concentration is much higher during  $\alpha$  pinene oxidation by  $O_3 + NO_3$  than during~~  
 485 ~~ozonolysis.~~



486  
 487 [Figure 6. Number and mass concentrations \(a\), as well as the size distribution \(b\) of particles formed](#)  
 488 [from the ozonolysis and synergistic  \$O\_3 + NO\_3\$  oxidation of  \$\alpha\$ -pinene \(Exps 13-14\).](#)

489



490

491 ~~Figure 6. Number and mass concentrations of particles formed from the ozonolysis and~~  
492 ~~synergistic O<sub>3</sub> + NO<sub>3</sub> oxidation of α-pinene (Exps 13-14).~~

### 493 3.4 Atmospheric relevance of experimental results

494 In the present study, the flow tube experiments were conducted under dry conditions. Although  
495 water vapor may affect the fate of Criegee intermediates (CIs) and RO<sub>2</sub> radicals and thereby HOM  
496 formation during the oxidation of organics under humid conditions, there is growing evidence that  
497 such effects in the α-pinene oxidation system are small. Kinetics studies have found that the  
498 stabilized Criegee intermediates (SCIs) arising from α-pinene ozonolysis can undergo fast  
499 unimolecular decay at a rate constant of 60 – 250 s<sup>-1</sup> (Vereecken et al., 2017; Newland et al., 2018),  
500 which is rapid compared to their reaction with water vapor, in particular for syn-SCIs, under  
501 atmospheric conditions (Vereecken et al., 2017; Newland et al., 2018). In addition, the yield of OH  
502 radicals from CI decomposition is independent of RH (Atkinson et al., 1992; Aschmann et al., 2002).  
503 Consistent with the fast unimolecular reaction kinetics revealed by these studies, recent laboratory  
504 measurements have shown that the contribution of SCIs to the formation of gas-phase and particle-  
505 phase dimers are small (<20%) during α-pinene ozonolysis (Zhao et al., 2018; Zhao et al., 2022).  
506 Furthermore, the molecular composition and abundance of HOM monomers and dimers (Li et al.,  
507 2019) and the formation of particle-phase dimers (Zhang et al., 2015; Kenseth et al., 2018) do not  
508 change significantly with RH ranging from 3% to 92%. These studies suggest that the humidity  
509 condition does not strongly affect the HOM formation chemistry in the α-pinene ozonolysis system.

510 To evaluate the relevance of our experimental findings to the real atmosphere, we performed

511 chemical model simulations of HOM formation from nocturnal synergistic O<sub>3</sub> + NO<sub>3</sub> oxidation of  
512 α-pinene under typical atmospheric conditions. In these simulations, constant concentrations of α-  
513 pinene (1 ppb), O<sub>3</sub> (30 ppb), NO (5 ppt), NO<sub>2</sub> (1.8 ppb), NO<sub>3</sub> radicals (0.2 or 1 ppt), OH radicals (5  
514 – 50 × 10<sup>4</sup> molecules cm<sup>-3</sup>), HO<sub>2</sub> radicals (4 ppt), as well as a constant RH of 50% and temperature  
515 of 298 K were used as typical nocturnal conditions in the boreal forest according to the field studies  
516 (Stone et al., 2012; Lee et al., 2016a; Brown and Stutz, 2012; Geyer et al., 2003b; Kristensen et al.,  
517 2016; Hakola et al., 2012; Liebmann et al., 2018). Considering the rapid deposition of oxidized  
518 biogenic compounds (Nguyen et al., 2015), a typical dilution lifetime of 5 h (i.e.,  $k_{\text{dil}} = 1/5 \text{ h}^{-1}$ ) was  
519 assumed in the model. According to the above analysis, the cross-reaction rate constants for <sup>NO<sub>3</sub></sup>RO<sub>2</sub>  
520 + <sup>Cl</sup>RO<sub>2</sub> and <sup>NO<sub>3</sub></sup>RO<sub>2</sub> + <sup>OH</sup>RO<sub>2</sub> were set to 1 × 10<sup>-12</sup> cm<sup>3</sup> molecule<sup>-1</sup> s<sup>-1</sup> and 1 × 10<sup>-13</sup> cm<sup>3</sup> molecule<sup>-1</sup>  
521 s<sup>-1</sup> in the model, respectively. The formation of RO<sub>2</sub> with oxygen numbers higher than 11 was not  
522 considered in the model, due to the large uncertainty in the autoxidation rate constants of the highly  
523 oxygenated RO<sub>2</sub>. In fact, the autoxidation rate of the highly oxygenated RO<sub>2</sub> is expected to be small  
524 given the significant decrease in the number of active sites for intramolecular H-abstraction in the  
525 molecule. As a result, the contribution of the most oxygenated HOMs to the total HOM monomers  
526 could be relatively small (Zhao et al., 2018; Clafin et al., 2018).

527 In the absence of NO<sub>3</sub> radicals (with NO<sub>3</sub> concentrations and formation rates set to zero), the amount  
528 of α-pinene consumed during 4 hours of simulation is 1.04 ppb. When a relatively low NO<sub>3</sub>  
529 concentration (0.2 ppt) is considered (Figure 7a), the amount of α-pinene consumed is 1.48 ppb, and  
530 the ozonolysis is the primary loss pathway of α-pinene (68%), followed by NO<sub>3</sub> (30%) and OH  
531 oxidation (2%). The reactions of RO<sub>2</sub> + HO<sub>2</sub>, RO<sub>2</sub> + NO, and RO<sub>2</sub> + RO<sub>2</sub> account for ~49%, ~27%,  
532 and ~24% of the total RO<sub>2</sub> fate, respectively (Figure S10a). Compared to the ozonolysis of α-pinene,  
533 the synergistic O<sub>3</sub> + NO<sub>3</sub> oxidation leads to a reduction of 3% and 13% in the formation of C<sub>x</sub>H<sub>y</sub>O<sub>z</sub>-  
534 HOM monomers and dimers, respectively (Figure 7b). Given that the concentrations of α-pinene  
535 and oxidants were held constant during the simulation, the consumptions of α-pinene by O<sub>3</sub> and OH  
536 radicals are the same across different oxidation regimes. Therefore, the decreases in the  
537 concentrations of C<sub>x</sub>H<sub>y</sub>O<sub>z</sub>-HOM monomers and dimers in the presence of NO<sub>3</sub> oxidation are mainly  
538 due to the cross reactions of <sup>NO<sub>3</sub></sup>RO<sub>2</sub> with other RO<sub>2</sub>. When the NO<sub>3</sub> concentration is as high as 1  
539 ppt as reported in field studies (Liebmann et al., 2018), the consumption of α-pinene reaches 3.24



540 ppb, of which 68% is contributed by NO<sub>3</sub> oxidation (Figure 7c). Under this condition, the RO<sub>2</sub> +  
541 RO<sub>2</sub> reactions account for ~34% of the total RO<sub>2</sub> fate (Figure S10b). As a result, the cross reactions  
542 of <sup>NO<sub>3</sub></sup>RO<sub>2</sub> with other RO<sub>2</sub> play a more important role in the HOM formation. The production of  
543 C<sub>x</sub>H<sub>y</sub>O<sub>z</sub>-HOM monomers and dimers decreases by 13% and 43%, respectively, due to the presence  
544 of NO<sub>3</sub> oxidation (Figure 7d). We note that the variation in RH from 0-90% in the model has negligible  
545 influence on the relative changes in C<sub>x</sub>H<sub>y</sub>O<sub>z</sub>-HOMs under these nocturnal atmospheric conditions (Figure  
546 S11). Considering that there are uncertainties in the dilution rate constant, a sensitivity analysis was  
547 performed by varying the *k*<sub>dil</sub> in the range of 0.04 – 0.2 h<sup>-1</sup>. It is found that the variation within these  
548 rate values does not significantly influence the response of C<sub>x</sub>H<sub>y</sub>O<sub>z</sub>-HOM dimer formation to  
549 concurrent NO<sub>3</sub> oxidation (Figure S12).

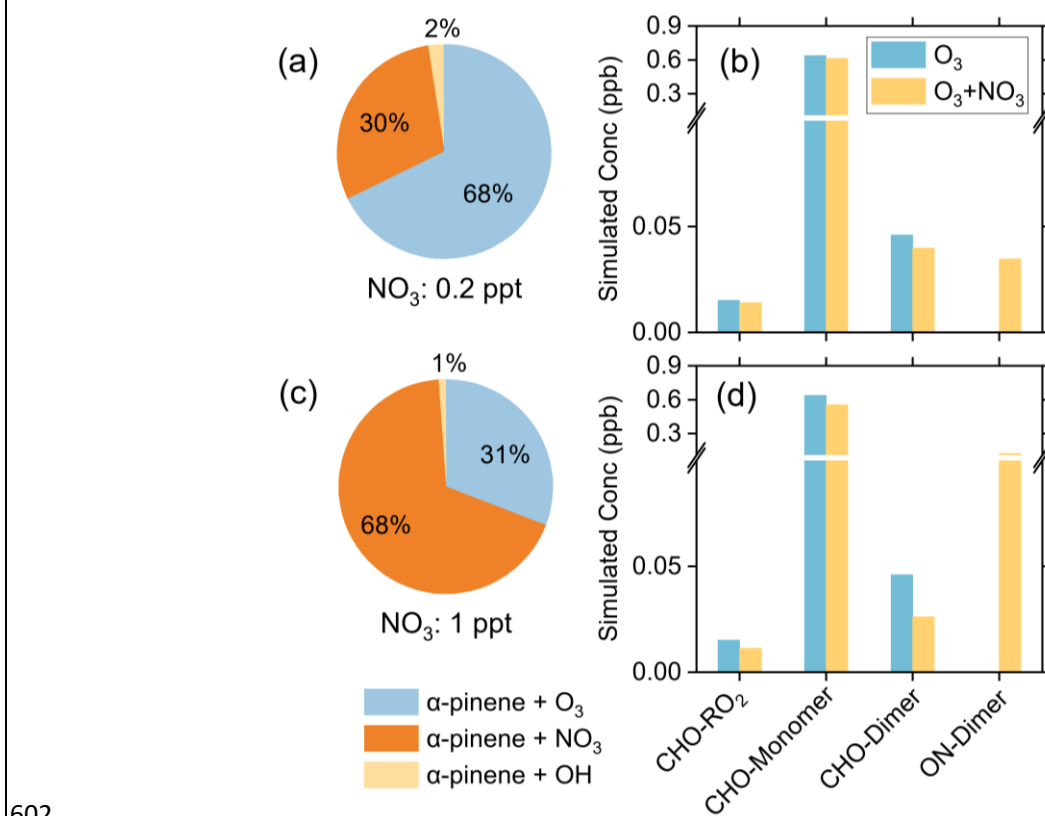
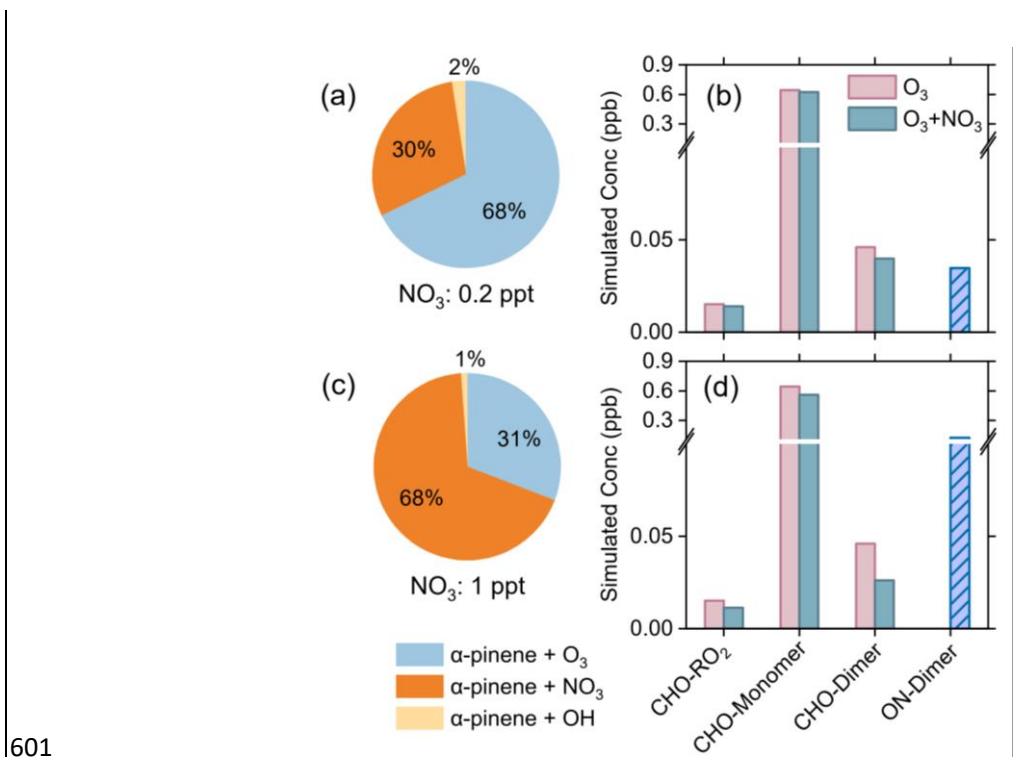
550 Field observations have shown that NO<sub>3</sub> radicals, O<sub>3</sub>, and OH radicals all had important  
551 contributions to monoterpene oxidation during the early morning after sunrise and late afternoon  
552 before sunset in the southeastern United States (Zhang et al., 2018). In addition, relatively high  
553 nighttime OH concentrations of (2 – 10) × 10<sup>5</sup> molecules cm<sup>-3</sup> were measured in some areas such  
554 as Germany and New York City (Faloona et al., 2001; Geyer et al., 2003a). As a result, a model  
555 simulation was conducted using a 10 times higher OH concentration (5 × 10<sup>5</sup> molecules cm<sup>-3</sup>). The  
556 concentration of NO<sub>3</sub> radicals is 1 ppt and the concentrations of other species are the same as the  
557 values mentioned above. With a higher OH concentration, O<sub>3</sub>, NO<sub>3</sub>, and OH radicals account for  
558 28%, 62%, and 10% to the total α-pinene consumption, respectively (Figure S13 a). Compared to  
559 the results under low OH concentration, the formation of C<sub>x</sub>H<sub>y</sub>O<sub>z</sub>-HOM monomers and dimers are  
560 all enhanced under high OH concentration (Figure S13 b). This is mainly due to the promoted  
561 self/cross reactions of <sup>OH</sup>RO<sub>2</sub>, as well as the promoted formation of C<sub>10</sub>H<sub>15</sub>O<sub>x</sub>-RO<sub>2</sub> derived from H-  
562 abstraction pathway by OH radicals. Nevertheless, the presence of NO<sub>3</sub> oxidation still reduces the  
563 formation of C<sub>x</sub>H<sub>y</sub>O<sub>z</sub>-HOM dimers by 26% (Figure S13 b). The same species concentration (NO<sub>3</sub>=  
564 1 ppt) as mentioned above but a 10 times higher OH concentration (5 × 10<sup>5</sup> molecules cm<sup>-3</sup>) were  
565 also conducted. With a higher OH concentration, O<sub>3</sub>, NO<sub>3</sub>, and OH radicals account for 28%, 62%,  
566 and 10% to the total α pinene consumption, respectively (Figure S6 S12 a). Compared to the results  
567 under low OH concentration, the formation of C<sub>x</sub>H<sub>y</sub>O<sub>z</sub>-HOM monomers and dimers are all enhanced  
568 under high OH concentration (Figure S6 S12 b). This is mainly due to the promoted self/cross-

569 reactions of  $^{\text{OH}}\text{RO}_2$ , as well as the promoted formation of  $\text{C}_{10}\text{H}_{15}\text{O}_x\text{-RO}_2$  derived from H-abstraction  
570 pathway by OH radicals. Nevertheless, the presence of  $\text{NO}_3$  oxidation still reduces the formation of  
571  $\text{C}_x\text{H}_y\text{O}_z$ -HOM dimers by 26% (Figure S6 S12 b).

572 Furthermore, model simulations for conditions typical of the southeastern United States (see details  
573 in Section S4) suggest that the coexistence of isoprene appears to exacerbate the suppression effect  
574 of synergistic oxidation on HOM formation from monoterpenes. As shown in Figure S14, in the  
575 absence of isoprene, the synergistic  $\text{O}_3 + \text{NO}_3$  oxidation of  $\alpha$ -pinene leads to a reduction of 13% and  
576 24% in the formation of  $\text{C}_x\text{H}_y\text{O}_z$ -HOM monomers and dimers, respectively. When isoprene is  
577 present, as the isoprene +  $\text{NO}_3$  oxidation produces a significant amount of nitrooxy  $\text{RO}_2$  that can  
578 also scavenge  $\alpha$ -pinene-derived  $^{\text{Cl}}\text{RO}_2$  and  $^{\text{OH}}\text{RO}_2$  via cross reactions, the synergistic oxidation leads  
579 to a slightly larger reduction in  $\text{C}_x\text{H}_y\text{O}_z$ -HOM monomers and dimers (15% and 31%, respectively).

580 The above model simulations suggest that under nocturnal atmospheric conditions with a very low  
581  $\text{NO}_3$  concentration, the  $\text{RO}_2$  radical pool is dominated by  $^{\text{Cl}}\text{RO}_2$  and their self/cross reactions are a  
582 major contributor to ULVOCs such as the highly oxygenated  $\text{C}_{20}$  dimers as observed in boreal forest  
583 (Bianchi et al., 2017). When the  $\text{NO}_3$  concentration is high, the production of  $^{\text{NO}_3}\text{RO}_2$  becomes  
584 significant and their cross reactions with  $^{\text{Cl}}\text{RO}_2$  would suppress the formation of ULVOCs. Although  
585 HOM-ON dimers are readily produced by cross reactions between  $^{\text{NO}_3}\text{RO}_2$  and  $^{\text{Cl}}\text{RO}_2$ , they generally  
586 have higher volatilities than  $\text{C}_x\text{H}_y\text{O}_z$ -HOM dimers and therefore are less efficient in initiating  
587 particle formation. However, these HOM-ONs can be an important contributor to the particle mass  
588 growth. As suggested by the model simulations in Bates et al. (2022), the  $\text{NO}_3$  oxidation of  $\alpha$ -pinene  
589 led to a particulate nitrate yield of 7% under nocturnal atmospheric conditions in rural Alabama  
590 during the SOAS campaign. The above model simulations clearly suggest that under typical  
591 nocturnal atmospheric conditions, the synergistic oxidation of  $\alpha$ -pinene by  $\text{O}_3$  and  $\text{NO}_3$  radicals can  
592 significantly inhibit the formation of  $\text{C}_x\text{H}_y\text{O}_z$ -HOMs, many of which are characterized as ULVOCs  
593 capable of driving particle nucleation and initial growth. Although HOM-ON dimers are readily  
594 produced by cross reactions between  $^{\text{NO}_3}\text{RO}_2$  and  $^{\text{Cl}}\text{RO}_2$ , they generally have higher volatilities than  
595  $\text{C}_x\text{H}_y\text{O}_z$ -HOM dimers and therefore are less efficient in initiating particle formation. Our results  
596 offer mechanistic and quantitative insights on how the synergistic oxidation of  $\alpha$ -pinene by  $\text{O}_3$  and  
597  $\text{NO}_3$  radicals can influence the formation of low-volatility organic compounds and hence particle

598 formation and growth. They also provide a potential explanation for field observations that NPF  
 599 events frequently occur in monoterpene-rich regions during daytime but not at nighttime (Mohr et  
 600 al., 2017; Kulmala et al., 2001; Junninen et al., 2017).



603 Figure 7. Model simulations of  $\alpha$ -pinene oxidation and HOM formation under typical nighttime

604 conditions in the boreal forest. (a, c) Contributions of different loss pathways of  $\alpha$ -pinene by  
605 different oxidants at  $\text{NO}_3$  concentrations of 0.2 and 1 ppt, respectively; (b, d) Concentrations of  
606  $\text{C}_x\text{H}_y\text{O}_z$ -HOMs and HOM-ONs formed by synergistic  $\text{O}_3 + \text{NO}_3$  oxidation and ozonolysis of  $\alpha$ -  
607 pinene under conditions corresponding to (a) and (c). The simulations were run for 4 h after an 8-h  
608 spin-up for intermediates and secondary species.

#### 609 4. Conclusions

610 This study provides a comprehensive characterization of the nocturnal synergistic oxidation of  $\alpha$ -  
611 pinene by  $\text{O}_3$  and  $\text{NO}_3$  radicals and its influence on the formation of HOMs and low-volatility  
612 organic compounds using a combination of flow reactor experiments and detailed kinetic model  
613 simulations. It is found that the formation of  $\text{C}_x\text{H}_y\text{O}_z$ -HOMs in the  $\text{O}_3 + \text{NO}_3$  regime is significantly  
614 suppressed compared to that in the  $\text{O}_3$ -only regime, mainly due to the ~~termination~~-depletion\_of  
615 ozonolysis-derived  $\text{RO}_2$  (i.e.,  $^{\text{Cl}}\text{RO}_2$  and  $^{\text{OH}}\text{RO}_2$ ) ~~by~~-by  $^{\text{NO}_3}\text{RO}_2$  via cross reactions. In addition, the  
616 decreases in the abundance of  $^{\text{Cl}}\text{RO}_2$  and related HOMs are significantly larger than those of OH-  
617 derived ones, indicating that the  $^{\text{NO}_3}\text{RO}_2$  species react more efficiently ~~on~~-with  $^{\text{Cl}}\text{RO}_2$  than ~~on~~-with  
618  $^{\text{OH}}\text{RO}_2$ . Detailed measurement-model comparisons for the distribution of a suite of  $^{\text{Cl}}\text{RO}_2$ ,  $^{\text{OH}}\text{RO}_2$ ,  
619 and associated HOMs across different oxidation regimes further reveal that the ~~terminations~~  
620 ~~reactions~~cross reactions between  $^{\text{Cl}}\text{RO}_2$  and  $^{\text{NO}_3}\text{RO}_2$  are averagely 10 – 100 times more efficient  
621 than those of  $^{\text{OH}}\text{RO}_2$  and  $^{\text{NO}_3}\text{RO}_2$ .

622 The suppressed formation of  $\text{C}_x\text{H}_y\text{O}_z$ -HOMs in the synergistic  $\text{O}_3 + \text{NO}_3$  regime results in a  
623 significant reduction in ULVOCs. Although substantial amounts of HOM-ONs are formed from the  
624 cross-~~reactions~~ between  $^{\text{NO}_3}\text{RO}_2$  and  $^{\text{Cl}}\text{RO}_2$  or  $^{\text{OH}}\text{RO}_2$  in the synergistic oxidation regime, they have  
625 higher volatilities and are less likely to participate in the formation and initial growth of new  
626 particles. As a result, in our experiment the formation of new particles in the synergistic oxidation  
627 regime is substantially inhibited compared to the  $\text{O}_3$ -only regime. Chemical model simulations  
628 further confirm that the synergistic oxidation of  $\alpha$ -pinene by  $\text{O}_3$  and  $\text{NO}_3$  radicals can significantly  
629 inhibit the formation of  $\text{C}_x\text{H}_y\text{O}_z$ -HOMs, especially the ultra-low volatility  $\text{C}_x\text{H}_y\text{O}_z$ -HOM dimers  
630 under typical nighttime atmospheric conditions. Our study sheds lights on the synergistic oxidation  
631 mechanism of biogenic emissions and underscores the importance of considering this chemistry for  
632 a better depiction of the formation of low-volatility organics and particles in the atmosphere.

633

634 *Data availability.* The data presented in this work are available upon request from the corresponding  
635 author.

636

637 *Author contributions.* YZ and HZ designed the study, HZ and DH performed the experiments. YZ  
638 and HZ analyzed the data, conducted model simulations, and wrote the paper. All other authors  
639 contributed to discussion and writing.

640 *Competing interests.* The authors declare no conflict of interest.

641

642 *Acknowledgments.* This work was supported by the National Natural Science Foundation  
643 of China (grants 22376137 and 22022607). Dan Dan Huang acknowledges the financial  
644 support from the Science and Technology Commission of Shanghai Municipality (grant  
645 21230711000).

## 646 **References**

647 Aschmann, S. M., Arey, J., and Atkinson, R.: OH radical formation from the gas-phase reactions of O<sub>3</sub>  
648 with a series of terpenes, *Atmos. Environ.*, 36, 4347-4355, [https://doi.org/10.1016/S1352-](https://doi.org/10.1016/S1352-2310(02)00355-2)  
649 [2310\(02\)00355-2](https://doi.org/10.1016/S1352-2310(02)00355-2), 2002.

650 Atkinson, R., Aschmann, S. M., Arey, J., and Shorees, B.: Formation of OH radicals in the gas-phase  
651 reactions of O<sub>3</sub> with a series of terpenes, *J. Geophys. Res.-Atmos.*, 97, 6065-6073,  
652 <https://doi.org/10.1029/92JD00062>, 1992.

653 Ayres, B. R., Allen, H. M., Draper, D. C., Brown, S. S., Wild, R. J., Jimenez, J. L., Day, D. A.,  
654 Campuzano-Jost, P., Hu, W., de Gouw, J., Koss, A., Cohen, R. C., Duffey, K. C., Romer, P.,  
655 Baumann, K., Edgerton, E., Takahama, S., Thornton, J. A., Lee, B. H., Lopez-Hilfiker, F. D., Mohr,  
656 C., Wennberg, P. O., Nguyen, T. B., Teng, A., Goldstein, A. H., Olson, K., and Fry, J. L.: Organic  
657 nitrate aerosol formation via NO<sub>3</sub> + biogenic volatile organic compounds in the southeastern United  
658 States, *Atmos. Chem. Phys.*, 15, 13377-13392, <https://doi.org/10.5194/acp-15-13377-2015>, 2015.

659 Bates, K. H., Burke, G. J. P., Cope, J. D., and Nguyen, T. B.: Secondary organic aerosol and organic  
660 nitrogen yields from the nitrate radical (NO<sub>3</sub>) oxidation of alpha-pinene from various RO<sub>2</sub> fates,  
661 *Atmos. Chem. Phys.*, 22, 1467-1482, <https://doi.org/10.5194/acp-22-1467-2022>, 2022.

662 Berndt, T.: Peroxy radical processes and product formation in the OH radical-initiated oxidation of alpha-  
663 pinene for near-atmospheric conditions, *J. Phys. Chem. A*, 125, 9151-9160,  
664 <https://doi.org/10.1021/acs.jpca.1c05576>, 2021.

665 Berndt, T., Mentler, B., Scholz, W., Fischer, L., Herrmann, H., Kulmala, M., and Hansel, A.: Accretion  
666 product formation from ozonolysis and OH radical reaction of alpha-pinene: mechanistic insight  
667 and the influence of isoprene and ethylene, *Environ. Sci. Technol.*, 52, 11069-11077,  
668 <https://doi.org/10.1021/acs.est.8b02210>, 2018a.

669 Berndt, T., Scholz, W., Mentler, B., Fischer, L., Herrmann, H., Kulmala, M., and Hansel, A.: Accretion  
670 product formation from self- and cross-reactions of RO<sub>2</sub> radicals in the atmosphere, *Angew. Chem.*  
671 *Int. Edit.*, 57, 3820-3824, <https://doi.org/10.1002/anie.201710989>, 2018b.

672 Berndt, T., Richters, S., Jokinen, T., Hyttinen, N., Kurtén, T., Otkjær, R. V., Kjaergaard, H. G., Stratmann,  
673 F., Herrmann, H., Sipilä, M., Kulmala, M., and Ehn, M.: Hydroxyl radical-induced formation of  
674 highly oxidized organic compounds, *Nat. Commun.*, 7, <https://doi.org/10.1038/ncomms13677>,

675 2016.

676 Bianchi, F., Garmash, O., He, X. C., Yan, C., Iyer, S., Rosendahl, I., Xu, Z. N., Rissanen, M. P., Riva, M.,  
677 Taipale, R., Sarnela, N., Petäjä, T., Worsnop, D. R., Kulmala, M., Ehn, M., and Junninen, H.: The  
678 role of highly oxygenated molecules (HOMs) in determining the composition of ambient ions in the  
679 boreal forest, *Atmos. Chem. Phys.*, 17, 13819-13831, <https://doi.org/10.5194/acp-17-13819-2017>,  
680 2017.

681 Bianchi, F., Kurtén, T., Riva, M., Mohr, C., Rissanen, M. P., Roldin, P., Berndt, T., Crouse, J. D.,  
682 Wennberg, P. O., Mentel, T. F., Wildt, J., Junninen, H., Jokinen, T., Kulmala, M., Worsnop, D. R.,  
683 Thornton, J. A., Donahue, N., Kjaergaard, H. G., and Ehn, M.: Highly oxygenated organic molecules  
684 (HOM) from gas-phase autoxidation involving peroxy radicals: a key contributor to atmospheric  
685 aerosol, *Chem. Rev.*, 119, 3472-3509, <https://doi.org/10.1021/acs.chemrev.8b00395>, 2019.

686 Boyd, C. M., Sanchez, J., Xu, L., Eugene, A. J., Nah, T., Tuet, W. Y., Guzman, M. I., and Ng, N. L.:  
687 Secondary organic aerosol formation from the  $\beta$ -pinene+NO<sub>3</sub> system: effect of humidity and peroxy  
688 radical fate, *Atmos. Chem. Phys.*, 15, 7497-7522, <https://doi.org/10.5194/acp-15-7497-2015>, 2015.

689 Brown, S. S. and Stutz, J.: Nighttime radical observations and chemistry, *Chem. Soc. Rev.*, 41,  
690 <https://doi.org/10.1039/c2cs35181a>, 2012.

691 Clafin, M. S., Krechmer, J. E., Hu, W., Jimenez, J. L., and Ziemann, P. J.: Functional group composition  
692 of secondary organic aerosol formed from ozonolysis of  $\alpha$ -pinene under high VOC and autoxidation  
693 conditions, *ACS Earth Space Chem.*, 2, 1196-1210,  
694 <https://doi.org/10.1021/acsearthspacechem.8b00117>, 2018.

695 Daumit, K. E., Kessler, S. H., and Kroll, J. H.: Average chemical properties and potential formation  
696 pathways of highly oxidized organic aerosol, *Faraday Discuss.*, 165,  
697 <https://doi.org/10.1039/c3fd00045a>, 2013.

698 Donahue, N. M., Epstein, S. A., Pandis, S. N., and Robinson, A. L.: A two-dimensional volatility basis  
699 set: 1. organic-aerosol mixing thermodynamics, *Atmos. Chem. Phys.*, 11, 3303-3318,  
700 <https://doi.org/10.5194/acp-11-3303-2011>, 2011.

701 Donahue, N. M., Henry, K. M., Mentel, T. F., Kiendler-Scharr, A., Spindler, C., Bohn, B., Brauers, T.,  
702 Dorn, H. P., Fuchs, H., Tillmann, R., Wahner, A., Saathoff, H., Naumann, K.-H., Möhler, O., Leisner,  
703 T., Müller, L., Reinnig, M.-C., Hoffmann, T., Salo, K., Hallquist, M., Frosch, M., Bilde, M.,  
704 Tritscher, T., Barmet, P., Praplan, A. P., DeCarlo, P. F., Dommen, J., Prévôt, A. S. H., and  
705 Baltensperger, U.: Aging of biogenic secondary organic aerosol via gas-phase OH radical reactions,  
706 *P. Natl. Acad. Sci. USA*, 109, 13503-13508, <https://doi.org/10.1073/pnas.1115186109>, 2012.

707 Ehn, M., Thornton, J. A., Kleist, E., Sipilä, M., Junninen, H., Pullinen, I., Springer, M., Rubach, F.,  
708 Tillmann, R., and Lee, B.: A large source of low-volatility secondary organic aerosol, *Nature*, 506,  
709 476-479, <https://doi.org/10.1038/nature13032>, 2014.

710 Faloon, I., Tan, D., Brune, W., Hurst, J., Barket, D., Couch, T. L., Shepson, P., Apel, E., Riemer, D.,  
711 Thornberry, T., Carroll, M. A., Sillman, S., Keeler, G. J., Sagady, J., Hooper, D., and Paterson, K.:  
712 Nighttime observations of anomalously high levels of hydroxyl radicals above a deciduous forest  
713 canopy, *J. Geophys. Res.-Atmos.*, 106, 24315-24333, <https://doi.org/10.1029/2000JD900691>, 2001.

714 Fry, J. L., Draper, D. C., Barsanti, K. C., Smith, J. N., Ortega, J., Winkler, P. M., Lawler, M. J., Brown,  
715 S. S., Edwards, P. M., Cohen, R. C., and Lee, L.: Secondary organic aerosol formation and organic  
716 nitrate yield from NO<sub>3</sub> oxidation of biogenic hydrocarbons, *Environ. Sci. Technol.*, 48, 11944-11953,  
717 <https://doi.org/10.1021/es502204x>, 2014.

718 Geyer, A., Bächmann, K., Hofzumahaus, A., Holland, F., Konrad, S., Klüpfel, T., Pätz, H. W., Perner, D.,

719 Mihelcic, D., Schäfer, H. J., Volz-Thomas, A., and Platt, U.: Nighttime formation of peroxy and  
720 hydroxyl radicals during the BERLIOZ campaign: Observations and modeling studies, *J. Geophys.*  
721 *Res.-Atmos.*, 108, <https://doi.org/10.1029/2001JD000656>, 2003a.

722 Geyer, A., Bächmann, K., Hofzumahaus, A., Holland, F., Konrad, S., Klüpfel, T., Pätz, H. W., Perner, D.,  
723 Mihelcic, D., Schäfer, H. J., Volz-Thomas, A., and Platt, U.: Nighttime formation of peroxy and  
724 hydroxyl radicals during the BERLIOZ campaign: Observations and modeling studies, *J. Geophys.*  
725 *Res.-Atmos.*, 108, <https://doi.org/10.1029/2001JD000656>, 2003b.

726 Hakola, H., Hellén, H., Hemmilä, M., Rinne, J., and Kulmala, M.: In situ measurements of volatile  
727 organic compounds in a boreal forest, *Atmos. Chem. Phys.*, 12, 11665-11678,  
728 <https://doi.org/10.5194/acp-12-11665-2012>, 2012.

729 Hallquist, M., Wängberg, I., Ljungström, E., Barnes, I., and Becker, K. H.: Aerosol and product yields  
730 from NO<sub>3</sub> radical-initiated oxidation of selected monoterpenes, *Environ. Sci. Technol.*, 33, 553-559,  
731 <https://doi.org/10.1021/es980292s>, 1999.

732 Huang, R. J., Zhang, Y., Bozzetti, C., Ho, K. F., Cao, J. J., Han, Y., Daellenbach, K. R., Slowik, J. G.,  
733 Platt, S. M., Canonaco, F., Zotter, P., Wolf, R., Pieber, S. M., Bruns, E. A., Crippa, M., Ciarelli, G.,  
734 Piazzalunga, A., Schwikowski, M., Abbazade, G., Schnelle-Kreis, J., Zimmermann, R., An, Z.,  
735 Szidat, S., Baltensperger, U., El Haddad, I., and Prevot, A. S.: High secondary aerosol contribution  
736 to particulate pollution during haze events in China, *Nature*, 514, 218-222, [10.1038/nature13774](https://doi.org/10.1038/nature13774),  
737 2014.

738 Huang, W., Saathoff, H., Shen, X., Ramisetty, R., Leisner, T., and Mohr, C.: Chemical characterization  
739 of highly functionalized organonitrates contributing to night-time organic aerosol mass loadings and  
740 particle growth, *Environ. Sci. Technol.*, 53, 1165-1174, <https://doi.org/10.1021/acs.est.8b05826>,  
741 2019.

742 Hyttinen, N., Kupiainen-Määttä, O., Rissanen, M. P., Muuronen, M., Ehn, M., and Kurtén, T.: Modeling  
743 the charging of highly oxidized cyclohexene ozonolysis products using nitrate-based chemical  
744 ionization, *J. Phys. Chem. A*, 119, 6339-6345, <https://doi.org/10.1021/acs.jpca.5b01818>, 2015.

745 Inomata, S.: New particle formation promoted by OH reactions during  $\alpha$ -pinene ozonolysis, *ACS Earth*  
746 *Space Chem.*, 5, 1929-1933, <https://doi.org/10.1021/acsearthspacechem.1c00142>, 2021.

747 Isaacman-VanWertz, G. and Aumont, B.: Impact of organic molecular structure on the estimation of  
748 atmospherically relevant physicochemical parameters, *Atmos. Chem. Phys.*, 21, 6541-6563,  
749 <https://doi.org/10.5194/acp-21-6541-2021>, 2021.

750 Iyer, S., Rissanen, M. P., Valiev, R., Barua, S., Krechmer, J. E., Thornton, J., Ehn, M., and Kurten, T.:  
751 Molecular mechanism for rapid autoxidation in alpha-pinene ozonolysis, *Nat. Commun.*, 12, 878,  
752 <https://doi.org/10.1038/s41467-021-21172-w>, 2021.

753 Jenkin, M., Young, J., and Rickard, A.: The MCM v3.3.1 degradation scheme for isoprene, *Atmos. Chem.*  
754 *Phys.*, 15, 11433-11459, <https://doi.org/10.5194/acp-15-11433-2015>, 2015.

755 Jokinen, T., Sipilä, M., Richters, S., Kerminen, V. M., Paasonen, P., Stratmann, F., Worsnop, D., Kulmala,  
756 M., Ehn, M., and Herrmann, H.: Rapid autoxidation forms highly oxidized RO<sub>2</sub> radicals in the  
757 atmosphere, *Angew. Chem. Int. Edit.*, 53, 14596-14600, <https://doi.org/10.1002/anie.201408566>,  
758 2014.

759 Junninen, H., Ehn, M., Petäjä, T., Luosujärvi, L., Kotiaho, T., Kostiaainen, R., Rohner, U., Gonin, M.,  
760 Fuhrer, K., and Kulmala, M.: A high-resolution mass spectrometer to measure atmospheric ion  
761 composition, *Atmos. Meas. Tech.*, 3, 1039-1053, <https://doi.org/10.5194/amt-3-1039-2010>, 2010.

762 Junninen, H., Hulkkonen, M., Riipinen, I., Nieminen, T., Hirsikko, A., Suni, T., Boy, M., Lee, S.-H., Vana,

763 M., Tammet, H., Kerminen, V.-M., and Kulmala, M.: Observations on nocturnal growth of  
764 atmospheric clusters, *Tellus B: Chemical and Physical Meteorology*, 60, 365-371,  
765 <https://doi.org/10.1111/j.1600-0889.2008.00356.x>, 2017.

766 Kenseth, C. M., Huang, Y., Zhao, R., Dalleska, N. F., Hethcox, J. C., Stoltz, B. M., and Seinfeld, J. H.:  
767 Synergistic O<sub>3</sub> + OH oxidation pathway to extremely low-volatility dimers revealed in beta-pinene  
768 secondary organic aerosol, *P. Natl. Acad. Sci. USA*, 115, 8301-8306,  
769 <https://doi.org/10.1073/pnas.1804671115>, 2018.

770 Kirkby, J., Duplissy, J., Sengupta, K., Frege, C., Gordon, H., Williamson, C., Heinritzi, M., Simon, M.,  
771 Yan, C., Almeida, J., Tröstl, J., Nieminen, T., Ortega, I. K., Wagner, R., Adamov, A., Amorim, A.,  
772 Bernhammer, A.-K., Bianchi, F., Breitenlechner, M., Brilke, S., Chen, X., Craven, J., Dias, A.,  
773 Ehrhart, S., Flagan, R. C., Franchin, A., Fuchs, C., Guida, R., Hakala, J., Hoyle, C. R., Jokinen, T.,  
774 Junninen, H., Kangasluoma, J., Kim, J., Krapf, M., Kürten, A., Laaksonen, A., Lehtipalo, K.,  
775 Makhmutov, V., Mathot, S., Molteni, U., Onnela, A., Peräkylä, O., Piel, F., Petäjä, T., Praplan, A. P.,  
776 Pringle, K., Rap, A., Richards, N. A. D., Riipinen, I., Rissanen, M. P., Rondo, L., Sarnela, N.,  
777 Schobesberger, S., Scott, C. E., Seinfeld, J. H., Sipilä, M., Steiner, G., Stozhkov, Y., Stratmann, F.,  
778 Tomé, A., Virtanen, A., Vogel, A. L., Wagner, A. C., Wagner, P. E., Weingartner, E., Wimmer, D.,  
779 Winkler, P. M., Ye, P., Zhang, X., Hansel, A., Dommen, J., Donahue, N. M., Worsnop, D. R.,  
780 Baltensperger, U., Kulmala, M., Carslaw, K. S., and Curtius, J.: Ion-induced nucleation of pure  
781 biogenic particles, *Nature*, 533, 521-526, <https://doi.org/10.1038/nature17953>, 2016.

782 Kristensen, K., Watne, Å. K., Hammes, J., Lutz, A., Petäjä, T., Hallquist, M., Bilde, M., and Glasius, M.:  
783 High-molecular weight dimer esters are major products in aerosols from  $\alpha$ -pinene ozonolysis and  
784 the boreal forest, *Environ. Sci. Tech. Lett.*, 3, 280-285, <https://doi.org/10.1021/acs.estlett.6b00152>,  
785 2016.

786 Kulmala, M., Hämeri, K., Aalto, P. P., Mäkelä, J. M., Pirjola, L., Nilsson, E. D., Buzorius, G., Rannik,  
787 Ü., Dal Maso, M., Seidl, W., Hoffman, T., Janson, R., Hansson, H. C., Viisanen, Y., Laaksonen, A.,  
788 and O'Dowd, C. D.: Overview of the international project on biogenic aerosol formation in the  
789 boreal forest (BIOFOR), *Tellus Series B-Chemical and Physical Meteorology*, 53, 324-343,  
790 <https://doi.org/10.1034/j.1600-0889.2001.530402.x>, 2001.

791 Kurtén, T., Møller, K. H., Nguyen, T. B., Schwantes, R. H., Misztal, P. K., Su, L., Wennberg, P. O., Fry,  
792 J. L., and Kjaergaard, H. G.: Alkoxy radical bond scissions explain the anomalously low secondary  
793 organic aerosol and organonitrate yields from  $\alpha$ -pinene + NO<sub>3</sub>, *J. Phys. Chem. L*, 8, 2826-2834,  
794 <https://doi.org/10.1021/acs.jpcllett.7b01038>, 2017.

795 Lee, B. H., D'Ambro, E. L., Lopez-Hilfiker, F. D., Schobesberger, S., Mohr, C., Zawadowicz, M. A., Liu,  
796 J., Shilling, J. E., Hu, W., Palm, B. B., Jimenez, J. L., Hao, L., Virtanen, A., Zhang, H., Goldstein,  
797 A. H., Pye, H. O. T., and Thornton, J. A.: Resolving ambient organic aerosol formation and aging  
798 pathways with simultaneous molecular composition and volatility observations, *ACS Earth Space*  
799 *Chem.*, 4, 391-402, <https://doi.org/10.1021/acsearthspacechem.9b00302>, 2020.

800 Lee, S. H., Uin, J., Guenther, A. B., de Gouw, J. A., Yu, F., Nadykto, A. B., Herb, J., Ng, N. L., Koss, A.,  
801 Brune, W. H., Baumann, K., Kanawade, V. P., Keutsch, F. N., Nenes, A., Olsen, K., Goldstein, A.,  
802 and Ouyang, Q.: Isoprene suppression of new particle formation: Potential mechanisms and  
803 implications, *J. Geophys. Res.-Atmos.*, 121, <https://doi.org/10.1002/2016jd024844>, 2016a.

804 Lee, S. H., Uin, J., Guenther, A. B., de Gouw, J. A., Yu, F. Q., Nadykto, A. B., Herb, J., Ng, N. L., Koss,  
805 A., Brune, W. H., Baumann, K., Kanawade, V. P., Keutsch, F. N., Nenes, A., Olsen, K., Goldstein,  
806 A., and Ouyang, Q.: Isoprene suppression of new particle formation: Potential mechanisms and



807 implications, *J. Geophys. Res.-Atmos.*, 121, 14621-14635, <https://doi.org/10.1002/2016jd024844>,  
808 2016b.

809 Li, D., Huang, W., Wang, D., Wang, M., Thornton, J. A., Caudillo, L., Rörup, B., Marten, R., Scholz, W.,  
810 Finkenzeller, H., Marie, G., Baltensperger, U., Bell, D. M., Brasseur, Z., Curtius, J., Dada, L.,  
811 Duplissy, J., Gong, X., Hansel, A., He, X.-C., Hofbauer, V., Junninen, H., Krechmer, J. E., Kürten,  
812 A., Lamkaddam, H., Lehtipalo, K., Lopez, B., Ma, Y., Mahfouz, N. G. A., Manninen, H. E., Mentler,  
813 B., Perrier, S., Petäjä, T., Pfeifer, J., Philippov, M., Schervish, M., Schobesberger, S., Shen, J., Surdu,  
814 M., Tomaz, S., Volkamer, R., Wang, X., Weber, S. K., Welti, A., Worsnop, D. R., Wu, Y., Yan, C.,  
815 Zauner-Wieczorek, M., Kulmala, M., Kirkby, J., Donahue, N. M., George, C., El-Haddad, I.,  
816 Bianchi, F., and Riva, M.: Nitrate radicals suppress biogenic new particle formation from  
817 monoterpene oxidation, *Environ. Sci. Technol.*, 58, 1601-1614,  
818 <https://doi.org/10.1021/acs.est.3c07958>, 2024.

819 Li, X. X., Chee, S., Hao, J. M., Abbatt, J. P. D., Jiang, J. K., and Smith, J. N.: Relative humidity effect  
820 on the formation of highly oxidized molecules and new particles during monoterpene oxidation,  
821 *Atmos. Chem. Phys.*, 19, 1555-1570, <https://doi.org/10.5194/acp-19-1555-2019>, 2019.

822 Li, Y., Pöschl, U., and Shiraiwa, M.: Molecular corridors and parameterizations of volatility in the  
823 chemical evolution of organic aerosols, *Atmos. Chem. Phys.*, 16, 3327-3344,  
824 <https://doi.org/10.5194/acp-16-3327-2016>, 2016.

825 Liebmann, J., Karu, E., Sobanski, N., Schuladen, J., Ehn, M., Schallhart, S., Quéléver, L., Hellen, H.,  
826 Hakola, H., Hoffmann, T., Williams, J., Fischer, H., Lelieveld, J., and Crowley, J. N.: Direct  
827 measurement of NO<sub>3</sub> radical reactivity in a boreal forest, *Atmos. Chem. Phys.*, 18, 3799-3815,  
828 <https://doi.org/10.5194/acp-18-3799-2018>, 2018.

829 Liu, J., D'Ambro, E. L., Lee, B. H., Schobesberger, S., Bell, D. M., Zaveri, R. A., Zelenyuk, A., Thornton,  
830 J. A., and Shilling, J. E.: Monoterpene photooxidation in a continuous-flow chamber: SOA yields  
831 and impacts of oxidants, NO(x), and VOC precursors, *Environ. Sci. Technol.*, 56, 12066-12076,  
832 <https://doi.org/10.1021/acs.est.2c02630>, 2022.

833 Martinez, E., Cabanas, B., Aranda, A., and Martin, P.: Kinetics of the reactions of NO<sub>3</sub> radical with  
834 selected monoterpenes: A temperature dependence study, *Environ. Sci. Technol.*, 32, 3730-3734,  
835 <https://doi.org/10.1021/es970899t>, 1998.

836 Mentel, T., Springer, M., Ehn, M., Kleist, E., Pullinen, I., Kurtén, T., Rissanen, M., Wahner, A., and Wildt,  
837 J.: Formation of highly oxidized multifunctional compounds: autoxidation of peroxy radicals  
838 formed in the ozonolysis of alkenes—deduced from structure—product relationships, *Atmos. Chem.*  
839 *Phys.*, 15, 6745-6765, <https://doi.org/10.5194/acp-15-6745-2015>, 2015.

840 Mohr, C., Lopez-Hilfiker, F. D., Yli-Juuti, T., Heitto, A., Lutz, A., Hallquist, M., D'Ambro, E. L.,  
841 Rissanen, M. P., Hao, L., Schobesberger, S., Kulmala, M., Mauldin, R. L., Makkonen, U., Sipilä,  
842 M., Petäjä, T., and Thornton, J. A.: Ambient observations of dimers from terpene oxidation in the  
843 gas phase: Implications for new particle formation and growth, *Geophysical Research Letters*, 44,  
844 2958-2966, [10.1002/2017gl072718](https://doi.org/10.1002/2017gl072718), 2017.

845 Molteni, U., Simon, M., Heinritzi, M., Hoyle, C. R., Bernhammer, A.-K., Bianchi, F., Breitenlechner, M.,  
846 Brilke, S., Dias, A., Duplissy, J., Frege, C., Gordon, H., Heyn, C., Jokinen, T., Kürten, A., Lehtipalo,  
847 K., Makhmutov, V., Petäjä, T., Pieber, S. M., Praplan, A. P., Schobesberger, S., Steiner, G., Stozhkov,  
848 Y., Tomé, A., Tröstl, J., Wagner, A. C., Wagner, R., Williamson, C., Yan, C., Baltensperger, U.,  
849 Curtius, J., Donahue, N. M., Hansel, A., Kirkby, J., Kulmala, M., Worsnop, D. R., and Dommen, J.:  
850 Formation of highly oxygenated organic molecules from  $\alpha$ -pinene ozonolysis: chemical

851 characteristics, mechanism, and kinetic model development, *ACS Earth Space Chem.*, 3, 873-883,  
852 <https://doi.org/10.1021/acsearthspacechem.9b00035>, 2019.

853 Mutzel, A., Zhang, Y., Böge, O., Rodigast, M., Kolodziejczyk, A., Wang, X., and Herrmann, H.:  
854 Importance of secondary organic aerosol formation of  $\alpha$ -pinene, limonene, and m-cresol comparing  
855 day- and nighttime radical chemistry, *Atmos. Chem. Phys.*, 21, 8479-8498,  
856 <https://doi.org/10.5194/acp-21-8479-2021>, 2021.

857 Newland, M. J., Rickard, A. R., Sherwen, T., Evans, M. J., Vereecken, L., Muñoz, A., Ródenas, M., and  
858 Bloss, W. J.: The atmospheric impacts of monoterpene ozonolysis on global stabilised Criegee  
859 intermediate budgets and SO<sub>2</sub> oxidation: experiment, theory and modelling, *Atmos. Chem. Phys.*,  
860 18, 6095-6120, <https://doi.org/10.5194/acp-18-6095-2018>, 2018.

861 Nguyen, T. B., Crounse, J. D., Teng, A. P., St. Clair, J. M., Paulot, F., Wolfe, G. M., and Wennberg, P. O.:  
862 Rapid deposition of oxidized biogenic compounds to a temperate forest, *P. Natl. Acad. Sci. USA*,  
863 112, <https://doi.org/10.1073/pnas.1418702112>, 2015.

864 Perraud, V., Bruns, E. A., Ezell, M. J., Johnson, S. N., Greaves, J., and Finlayson-Pitts\*, B. J.:  
865 Identification of organic nitrates in the NO<sub>3</sub> radical initiated oxidation of  $\alpha$ -pinene by atmospheric  
866 pressure chemical ionization mass spectrometry, *Environ. Sci. Technol.*, 44, 5887-5893,  
867 <https://doi.org/10.1021/es1005658>, 2010.

868 Pye, H. O. T., Ward-Caviness, C. K., Murphy, B. N., Appel, K. W., and Seltzer, K. M.: Secondary organic  
869 aerosol association with cardiorespiratory disease mortality in the United States, *Nat. Commun.*, 12,  
870 <https://doi.org/10.1038/s41467-021-27484-1>, 2021.

871 Schervish, M. and Donahue, N. M.: Peroxy radical chemistry and the volatility basis set, *Atmos. Chem.*  
872 *Phys.*, 20, 1183-1199, <https://doi.org/10.5194/acp-20-1183-2020>, 2020.

873 Shen, H., Vereecken, L., Kang, S., Pullinen, I., Fuchs, H., Zhao, D., and Mentel, T. F.: Unexpected  
874 significance of a minor reaction pathway in daytime formation of biogenic highly oxygenated  
875 organic compounds, *Sci. Adv.*, 8, eabp8702, <https://doi.org/10.1126/sciadv.abp8702>, 2022.

876 Shrivastava, M., Cappa, C. D., Fan, J., Goldstein, A. H., Guenther, A. B., Jimenez, J. L., Kuang, C.,  
877 Laskin, A., Martin, S. T., Ng, N. L., Petaja, T., Pierce, J. R., Rasch, P. J., Roldin, P., Seinfeld, J. H.,  
878 Shilling, J., Smith, J. N., Thornton, J. A., Volkamer, R., Wang, J., Worsnop, D. R., Zaveri, R. A.,  
879 Zelenyuk, A., and Zhang, Q.: Recent advances in understanding secondary organic aerosol:  
880 Implications for global climate forcing, *Reviews of Geophysics*, 55, 509-559,  
881 [10.1002/2016rg000540](https://doi.org/10.1002/2016rg000540), 2017.

882 Simon, M., Dada, L., Heinritzi, M., Scholz, W., Stolzenburg, D., Fischer, L., Wagner, A. C., Kürten, A.,  
883 Rörup, B., He, X.-C., Almeida, J., Baalbaki, R., Baccarini, A., Bauer, P. S., Beck, L., Bergen, A.,  
884 Bianchi, F., Bräkling, S., Brilke, S., Caudillo, L., Chen, D., Chu, B., Dias, A., Draper, D. C., Duplissy,  
885 J., El-Haddad, I., Finkenzeller, H., Frege, C., Gonzalez-Carracedo, L., Gordon, H., Granzin, M.,  
886 Hakala, J., Hofbauer, V., Hoyle, C. R., Kim, C., Kong, W., Lamkaddam, H., Lee, C. P., Lehtipalo,  
887 K., Leiminger, M., Mai, H., Manninen, H. E., Marie, G., Marten, R., Mentler, B., Molteni, U.,  
888 Nichman, L., Nie, W., Ojdanic, A., Onnela, A., Partoll, E., Petäjä, T., Pfeifer, J., Philippov, M.,  
889 Quéléver, L. L. J., Ranjithkumar, A., Rissanen, M. P., Schallhart, S., Schobesberger, S., Schuchmann,  
890 S., Shen, J., Sipilä, M., Steiner, G., Stozhkov, Y., Tauber, C., Tham, Y. J., Tomé, A. R., Vazquez-  
891 Pufleau, M., Vogel, A. L., Wagner, R., Wang, M., Wang, D. S., Wang, Y., Weber, S. K., Wu, Y., Xiao,  
892 M., Yan, C., Ye, P., Ye, Q., Zauner-Wieczorek, M., Zhou, X., Baltensperger, U., Dommen, J., Flagan,  
893 R. C., Hansel, A., Kulmala, M., Volkamer, R., Winkler, P. M., Worsnop, D. R., Donahue, N. M.,  
894 Kirkby, J., and Curtius, J.: Molecular understanding of new-particle formation from  $\alpha$ -pinene

895 between  $-50$  and  $+25$  °C, *Atmos. Chem. Phys.*, 20, 9183-9207, <https://doi.org/10.5194/acp-20->  
896 9183-2020, 2020.

897 Stone, D., Whalley, L. K., and Heard, D. E.: Tropospheric OH and HO<sub>2</sub> radicals: field measurements and  
898 model comparisons, *Chem. Soc. Rev.*, 41, <https://doi.org/10.1039/c2cs35140d>, 2012.

899 Vereecken, L., Novelli, A., and Taraborrelli, D.: Unimolecular decay strongly limits the atmospheric  
900 impact of Criegee intermediates, *Phys. Chem. Chem. Phys.*, 19, 31599-31612,  
901 <https://doi.org/10.1039/c7cp05541b>, 2017.

902 Wang, Y., Zhao, Y., Li, Z., Li, C., Yan, N., and Xiao, H.: Importance of hydroxyl radical chemistry in  
903 isoprene suppression of particle formation from  $\alpha$ -pinene ozonolysis, *ACS Earth Space Chem.*, 5,  
904 487-499, <https://doi.org/10.1021/acsearthspacechem.0c00294>, 2021.

905 Wolfe, G. M., Marvin, M. R., Roberts, S. J., Travis, K. R., and Liao, J.: The framework for 0-D  
906 atmospheric modeling (F0AM) v3. 1, *Geosci. Model Dev.*, 9, 3309-3319,  
907 <https://doi.org/10.5194/gmd-9-3309-2016>, 2016.

908 Xu, L., Møller, K. H., Crounse, J. D., Otkjær, R. V., Kjaergaard, H. G., and Wennberg, P. O.:  
909 Unimolecular reactions of peroxy radicals formed in the oxidation of  $\alpha$ -pinene and  $\beta$ -pinene by  
910 hydroxyl radicals, *J. Phys. Chem. A*, 123, 1661-1674, <https://doi.org/10.1021/acs.jpca.8b11726>,  
911 2019.

912 Zang, H., Huang, D., Zhong, J., Li, Z., Li, C., Xiao, H., and Zhao, Y.: Direct probing of acylperoxy  
913 radicals during ozonolysis of  $\alpha$ -pinene: constraints on radical chemistry and production of highly  
914 oxygenated organic molecules, *Atmos. Chem. Phys.*, 23, 12691-12705, <https://doi.org/10.5194/acp->  
915 23-12691-2023, 2023.

916 Zhang, H., Yee, L. D., Lee, B. H., Curtis, M. P., Worton, D. R., Isaacman-VanWertz, G., Offenberg, J. H.,  
917 Lewandowski, M., Kleindienst, T. E., Beaver, M. R., Holder, A. L., Lonneman, W. A., Docherty, K.  
918 S., Jaoui, M., Pye, H. O. T., Hu, W., Day, D. A., Campuzano-Jost, P., Jimenez, J. L., Guo, H., Weber,  
919 R. J., de Gouw, J., Koss, A. R., Edgerton, E. S., Brune, W., Mohr, C., Lopez-Hilfiker, F. D., Lutz,  
920 A., Kreisberg, N. M., Spielman, S. R., Hering, S. V., Wilson, K. R., Thornton, J. A., and Goldstein,  
921 A. H.: Monoterpenes are the largest source of summertime organic aerosol in the southeastern  
922 United States, *P. Natl. Acad. Sci. USA*, 115, 2038-2043, <https://doi.org/10.1073/pnas.1717513115>,  
923 2018.

924 Zhang, X., McVay, R. C., Huang, D. D., Dalleska, N. F., Aumont, B., Flagan, R. C., and Seinfeld, J. H.:  
925 Formation and evolution of molecular products in  $\alpha$ -pinene secondary organic aerosol, *P. Natl. Acad.*  
926 *Sci. USA*, 112, 14168-14173, <https://doi.org/10.1073/pnas.1517742112>, 2015.

927 Zhang, Y., Peräkylä, O., Yan, C., Heikkinen, L., Äijälä, M., Daellenbach, K. R., Zha, Q., Riva, M.,  
928 Garmash, O., Junninen, H., Paatero, P., Worsnop, D., and Ehn, M.: Insights into atmospheric  
929 oxidation processes by performing factor analyses on subranges of mass spectra, *Atmos. Chem.*  
930 *Phys.*, 20, 5945-5961, <https://doi.org/10.5194/acp-20-5945-2020>, 2020.

931 Zhao, Y., Thornton, J. A., and Pye, H. O. T.: Quantitative constraints on autoxidation and dimer formation  
932 from direct probing of monoterpene-derived peroxy radical chemistry, *P. Natl. Acad. Sci. USA*, 115,  
933 12142-12147, <https://doi.org/10.1073/pnas.1812147115>, 2018.

934 Zhao, Y., Yao, M., Wang, Y., Li, Z., Wang, S., Li, C., and Xiao, H.: Acylperoxy radicals as key  
935 intermediates in the formation of dimeric compounds in  $\alpha$ -pinene secondary organic aerosol,  
936 *Environ. Sci. Technol.*, 56, 14249-14261, <https://doi.org/10.1021/acs.est.2c02090>, 2022.

937 Zhao, Z., Zhang, W., Alexander, T., Zhang, X., Martin, D. B. C., and Zhang, H.: Isolating alpha-pinene  
938 ozonolysis pathways reveals new insights into peroxy radical chemistry and secondary organic

939 aerosol formation, Environ. Sci. Technol., 55, 6700-6709, <https://doi.org/10.1021/acs.est.1c02107>,  
940 2021.  
941